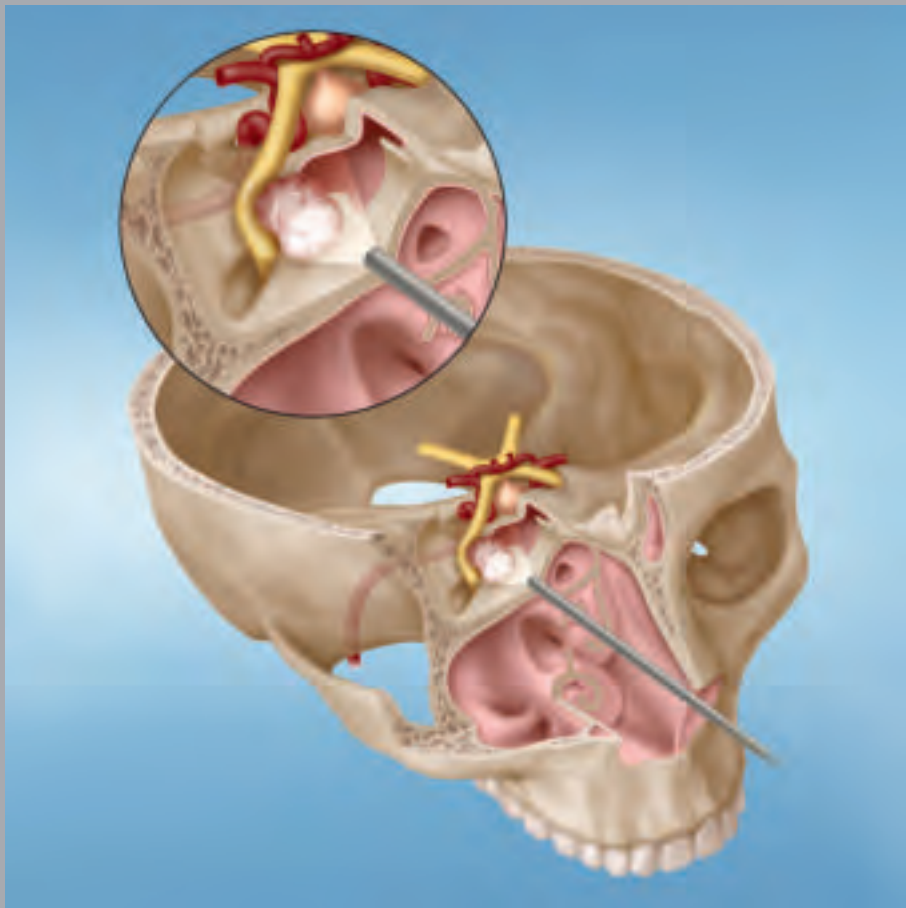


Endo:Press®

**PEDIATRIC ENDONASAL  
ENDOSCOPIC SKULL BASE SURGERY**  
A Case-Based Manual



Harminder SINGH  
Jeffrey P. GREENFIELD  
Vijay K. ANAND  
Theodore H. SCHWARTZ



# PEDIATRIC ENDONASAL ENDOSCOPIC SKULL BASE SURGERY

## A Case-Based Manual

Harminder SINGH, MD<sup>1</sup>  
Jeffrey P. GREENFIELD, MD, PhD<sup>2</sup>  
Vijay K. ANAND, MD<sup>3</sup>  
Theodore H. SCHWARTZ, MD<sup>4</sup>

<sup>1</sup>| Clinical Assistant Professor of Neurosurgery  
Stanford University School of Medicine  
Stanford University Medical Center

<sup>2</sup>| Associate Professor of Neurosurgery and Pediatrics  
Weill Cornell Medical College  
New York Presbyterian Hospital

<sup>3</sup>| Clinical Professor of Otorhinolaryngology  
Co-Director, Institute for Minimally Invasive  
Skull Base and Pituitary Surgery  
Weill Cornell Medical College  
New York Presbyterian Hospital

<sup>4</sup>| *David and Ursel Barnes* Professor of  
Minimally Invasive Neurosurgery  
Co-Director, Institute for Minimally Invasive  
Skull Base and Pituitary Surgery  
Weill Cornell Medical College  
New York Presbyterian Hospital



# Acknowledgements

We are indebted to our families  
for their enduring support and  
our patients for their trust.

**Illustrations:****Matthew Holt**

E-mail: matthew@bodyrender.com

www.bodyrender.com

**Pediatric Endonasal Endoscopic Skull Base Surgery – A Case-Based Manual****Harminder Singh, MD<sup>1</sup>****Jeffrey P. Greenfield, MD, PhD<sup>2</sup>****Vijay K. Anand, MD<sup>3</sup>****Theodore H. Schwartz, MD<sup>4</sup>**<sup>1</sup> Clinical Assistant Professor of Neurosurgery  
Stanford University School of Medicine  
Stanford University Medical Center<sup>2</sup> Associate Professor of Neurosurgery and Pediatrics  
Weill Cornell Medical College  
New York Presbyterian Hospital<sup>3</sup> Clinical Professor of Otorhinolaryngology  
Co-Director, Institute for Minimally Invasive Skull Base and  
Pituitary Surgery, Weill Cornell Medical College  
New York Presbyterian Hospital<sup>4</sup> David and Ursel Barnes Professor of Minimally Invasive  
Neurosurgery, Co-Director, Institute for Minimally Invasive  
Skull Base and Pituitary Surgery  
Weill Cornell Medical College New York Presbyterian Hospital**Important notes:**

Medical knowledge is ever changing. As new research and clinical experience broaden our knowledge, changes in treatment and therapy may be required. The authors and editors of the material herein have consulted sources believed to be reliable in their efforts to provide information that is complete and in accord with the standards accepted at the time of publication. However, in view of the possibility of human error by the authors, editors, or publisher, or changes in medical knowledge, neither the authors, editors, publisher, nor any other party who has been involved in the preparation of this booklet, warrants that the information contained herein is in every respect accurate or complete, and they are not responsible for any errors or omissions or for the results obtained from use of such information. The information contained within this booklet is intended for use by doctors and other health care professionals. This material is not intended for use as a basis for treatment decisions, and is not a substitute for professional consultation and/or use of peer-reviewed medical literature.

Some of the product names, patents, and registered designs referred to in this booklet are in fact registered trademarks or proprietary names even though specific reference to this fact is not always made in the text. Therefore, the appearance of a name without designation as proprietary is not to be construed as a representation by the publisher that it is in the public domain.

The use of this booklet as well as any implementation of the information contained within explicitly takes place at the reader's own risk. No liability shall be accepted and no guarantee is given for the work neither from the publisher or the editor nor from the author or any other party who has been involved in the preparation of this work. This particularly applies to the content, the timeliness, the correctness, the completeness as well as to the quality. Printing errors and omissions cannot be completely excluded. The publisher as well as the author or other copyright holders of this work disclaim any liability, particularly for any damages arising out of or associated with the use of the medical procedures mentioned within this booklet.

Any legal claims or claims for damages are excluded.

In case any references are made in this booklet to any 3<sup>rd</sup> party publication(s) or links to any 3<sup>rd</sup> party websites are mentioned, it is made clear that neither the publisher nor the author or other copyright holders of this booklet endorse in any way the content of said publication(s) and/or web sites referred to or linked from this booklet and do not assume any form of liability for any factual inaccuracies or breaches of law which may occur therein. Thus, no liability shall be accepted for content within the 3<sup>rd</sup> party publication(s) or 3<sup>rd</sup> party websites and no guarantee is given for any other work or any other websites at all.

**Correspondence address of the first author:****Harminder Singh, MD**

Clinical Assistant Professor of Neurosurgery

Stanford University School of Medicine

Stanford University Medical Center

300 Pasteur Dr,

Stanford, CA 94305, U.S.A.

E-mail: Harmansingh.md@gmail.com

All rights reserved.

1<sup>st</sup> edition

© 2016 Endo : Press® GmbH

P.O. Box, 78503 Tuttlingen, Germany

Phone: +49 (0) 74 61/1 45 90

Fax: +49 (0) 74 61/708-529

E-mail: endopress@t-online.de

No part of this publication may be translated, reprinted or reproduced, transmitted in any form or by any means, electronic or mechanical, now known or hereafter invented, including photocopying and recording, or utilized in any information storage or retrieval system without the prior written permission of the copyright holder.

Editions in languages other than English and German are in preparation. For up-to-date information, please contact Endo : Press® GmbH at the address shown above.

**Design and Composing:**

Endo : Press® GmbH, Germany

**Printing and Binding:**

Straub Druck + Medien AG

Max-Planck-Straße 17, 78713 Schramberg, Germany

09.16-1.5

**ISBN 978-3-89756-811-2**

# Table of Contents

<b>1</b>	<b>Introduction</b> .....	9
<b>2</b>	<b>Anatomy of the Developing Pediatric Skull Base and Implications for Endoscopic Endonasal Surgery</b> .....	9
2.1	Forces Driving Development .....	9
2.2	Age-Dependent Height, Length and Width of the Sphenoid Sinus ...	10
2.3	Sphenoidal Pneumatization Patterns. ....	11
	Sagittal plane .....	11
	Coronal plane .....	11
	Age-dependent Sphenoid Pneumatization Patterns .....	12
2.4	Inter-Carotid Distance (ICD) .....	12
2.5	Pediatric Naso-Septal Flap Harvest .....	13
<b>3</b>	<b>Pathology Unique to the Pediatric Skull Base</b> .....	13
3.1	Craniopharyngioma .....	13
3.2	Chiasmatic Glioma .....	13
3.3	Germ Cell Tumors .....	14
3.4	Juvenile Angiofibroma .....	14
3.5	Basilar Invagination/Platybasia .....	14
<b>4</b>	<b>Operating Room Set-Up</b> .....	15
4.1	Endonasal Approach with Intraoperative Image Guidance Using Preoperative Magnetic Resonance Imaging (MRI) .....	15
4.2	Endonasal Approach with Image Guidance Using Live Intraoperative Computed Tomography (CT) .....	15
<b>5</b>	<b>Endonasal Corridors and Approaches</b> .....	16
5.1	Transnasal and Transfrontal .....	16
5.2	Transsphenoidal .....	16
5.3	Transethmoidal .....	17
5.4	Transmaxillary .....	17
<b>6</b>	<b>Surgical Approaches – Clinical Cases and Operative Images</b> .....	18
6.1	Transtuberculum Approach for Craniopharyngioma .....	18
6.2	Transplanum Approach for Juvenile Pilocytic Astrocytoma (JPA) ...	20
6.3	Transcavernous Approach for Dermoid .....	22
6.4	Transcribriform Approach for Meningoencephalocele .....	24
6.5	Transclival Approach for Ependymoma .....	26
6.6	Transodontoid Approach for Basilar Invagination .....	28
6.7	Transorbital Approach for Rhabdomyosarcoma .....	30
6.8	Transpterygoid Approach for Juvenile Nasopharyngeal Angiofibroma (JNA) .....	32
	<b>Recommended Reading</b> .....	34
	<b>Recommended Instrumentation and Video Equipment for Pediatric Endonasal Endoscopic Skull Base Surgery</b> .....	36

## Contributing Authors



Dr. **Harminder Singh** graduated from University of Arizona Summa Cum Laude with Honors in Biology before receiving his M.D. from Tufts University School of Medicine. Following completion of his neurosurgical residency and chief residency at Thomas Jefferson University Hospital in Philadelphia, Dr. Singh received further training in minimally invasive skull base surgery at New York-Presbyterian Hospital/Weill Cornell Medical Center working with Dr. Theodore H. Schwartz and Vijay K. Anand. He also completed a complex cerebrovascular and skull base fellowship with Dr. Laligam Sekhar at University of Washington.

He has a special interest in applying the principles of minimally invasive surgery to treat neuro-oncologic disorders of the brain and spine. He is an Assistant Professor of Neurosurgery at Stanford University School of Medicine and Director of the Stanford Neuroanatomy and Simulation Laboratory.



Dr. **Jeffrey P. Greenfield** graduated from Amherst College Magna Cum Laude in Neuroscience before receiving his M.D. and Ph.D. degrees from the Weill Medical College of Cornell University. Following completion of his neurosurgical residency and chief residency at New York-Presbyterian Hospital/Weill Cornell Medical Center, Dr. Greenfield received further training in pediatric neurosurgery and the surgical treatment of brain tumors, epilepsy, spinal dysraphism, complex spinal column injury, spinal cord tumors, and fetal surgery for myelomeningocele at The Children's Hospital of Philadelphia.

He has a special interest in minimally invasive endoscopic approaches that are less traumatic than traditional surgery for his young patients and their families. He directs the pediatric skull base surgery, chiari, and spasticity surgery programs at Cornell.



Dr. **Vijay K. Anand** is a world-renowned endoscopic sinus surgeon who was instrumental in developing image guidance in endoscopic sinus surgery and anterior skull base surgery. He was the President of the American Rhinologic Society in 1995 and has been a pioneer in the development of endoscopic sinus surgery and its extended applications. He has published widely in the field of Rhinology and is the author of the Textbook on Practical Endoscopic Sinus Surgery. He is the recipient of the Outstanding Teacher Award in Rhinology from the American Rhinological Society.

He is a sought after speaker in the field of Rhinology and is a Clinical Professor of Otolaryngology at the Weill Medical College of Cornell University in New York as well as co-director of the Institute for Minimally Invasive Skull Base and Pituitary Surgery.



Dr. **Theodore H. Schwartz** received his undergraduate and medical degrees from Harvard University where he graduated Magna Cum Laude. After completing his residency and chief residency in Neurosurgery at The Neurological Institute of New York at Columbia-Presbyterian Medical Center, Dr. Schwartz completed advanced fellowship training at Yale-New Haven Medical Center in the surgical treatment of brain tumors and epilepsy. Dr. Schwartz specializes in image-guided minimally invasive surgical techniques such as stereotaxis, brain mapping and endoscopy. In 2014, Dr. Schwartz received the first endowed professorship in the Department of Neurosurgery at Weill Cornell Medical College, being named the *David and Ursel Barnes* Professor of Minimally Invasive Neurosurgery. He is the surgical director of the Comprehensive Epilepsy Center, as well as co-director of the Institute for Minimally Invasive Skull Base and Pituitary Surgery.

## 1

## Introduction

Endonasal skull base surgery has become widely accepted as a technique to manage adult skull base tumors, however, there has been limited work done in the pediatric population. Pediatric sinonasal and cranial base anatomy is much more restricted than in adult patients and the pathology encountered is often unique to the pediatric population. The narrower corridor afforded by the developing sino-nasal tract renders these approaches more challenging. Specially adapted micro-instruments that are now available permit passage through the narrow sinonasal pathway to access the entire midline skull base in a rostro-caudal fashion, from the crista galli to the cervico-medullary junction. In light of advancements in technology, expanded endonasal approaches (EEA) offer a new surgical paradigm to treat central skull base lesions in the pediatric population.

At Weill Cornell Medical College, the pediatric endonasal endoscopic skull base program was founded upon a collaboration between pediatric neurosurgery and the adult endoscopic skull base program. Our experience has shown the value of these approaches in managing a variety of skull base lesions in the pediatric population, and narrow pediatric corridors have not been a significant limitation. In light of our experience, we felt there was a need for a guide specifically geared to the endoscopic management of pediatric pathology and dealing with the anatomic constraints unique to the developing skull base.

This technical manual provides a practical guide to this subspecialty of pediatric endoscopic skull base surgery. In the context of cases presented from our clinical series, the manual will provide the reader with a discussion of operative nuances and instrumentation necessary to perform such surgery safely.

## 2

## Anatomy of the Developing Pediatric Skull Base and Implications for Endoscopic Endonasal Surgery

The development of the pediatric skull base is asynchronous and asymmetric. It is a gradual, age-dependent, sex-independent process that significantly alters endonasal endoscopic corridors. Anterior portions of the skull

base continue to expand over the entire childhood, while posterior areas finish the growth process earlier; inferiorly, pneumatization occurs in a lateral direction while frontal lobe growth models the anterior skull base from above.

### 2.1 Forces Driving Development

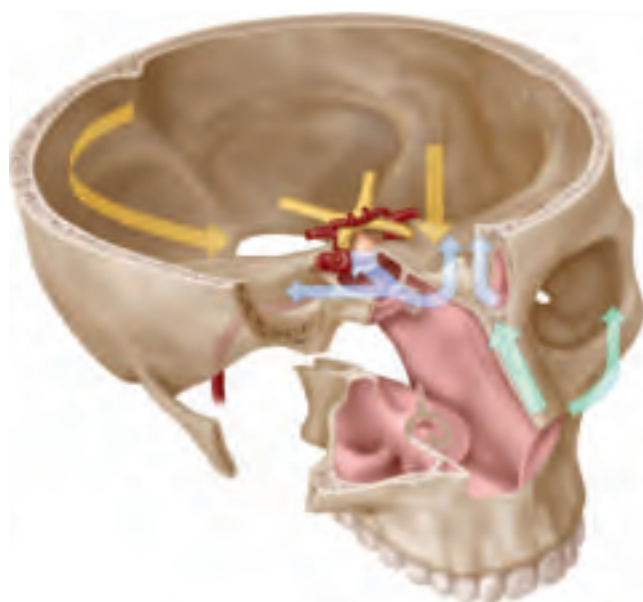


**Fig. 2.1** Frontal and temporal lobe development (yellow). Sphenoid sinus and frontal sinus pneumatization (blue). Development of the midfacial maxillary complex (green).

Sequential pneumatization of the sphenoid sinus occurs in an anterior to posterior and caudal to cranial fashion. This has an effect on neurovascular structures adjacent to the sella turcica – it pushes the internal carotid arteries laterally (red arrow) and the optic chiasm cranially (yellow arrow), opening up new endoscopic corridors.

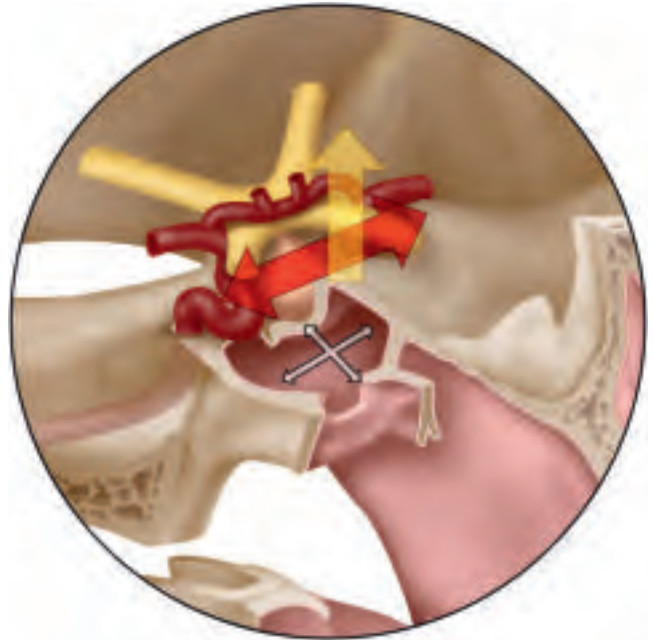


**Fig. 2.2** Sequential pneumatization of the sphenoid sinus. Internal carotid arteries (red arrow). Optic chiasm (yellow arrow).

## 2.2 Age-Dependent Height, Length and Width of the Sphenoid Sinus

The height, length and width of the sphenoid sinus increases with age. The extent of sphenoidal pneumatization directly impacts the amount of drilling necessary to reach the sella. Furthermore, as pneumatization extends laterally, new parasellar corridors become available.

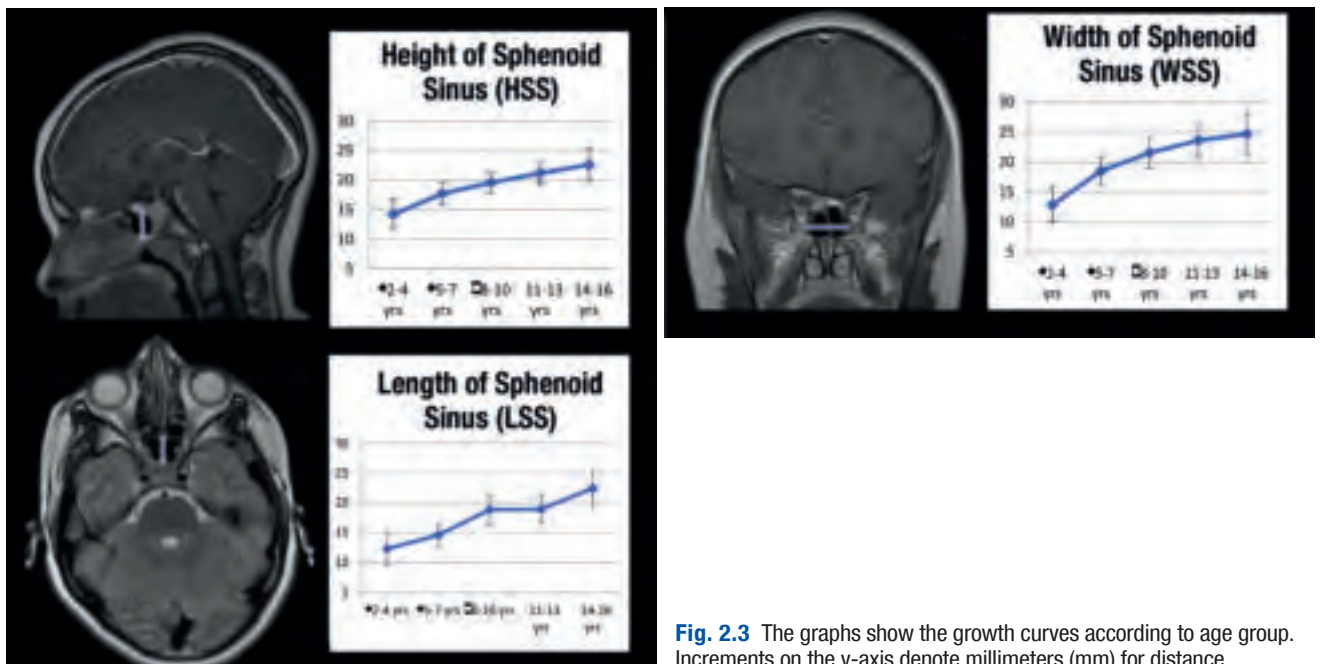


**Fig. 2.3** The graphs show the growth curves according to age group. Increments on the y-axis denote millimeters (mm) for distance.

## 2.3 Sphenoidal Pneumatization Patterns

Several different pneumatization patterns of the sphenoid have been described.

### Sagittal Plane



**Fig. 2.4**

- Type 1 **Conchal** (completely missing or minimal sphenoid sinus) (a).  
 Type 2 **Presellar** (posterior wall of sphenoid sinus is in front of the anterior wall of the sella) (b).  
 Type 3 **Sellar** (posterior wall of sphenoid sinus is between anterior and posterior wall of sella) (c).  
 Type 4A **Postsellar** (posterior wall of sphenoid sinus is behind the posterior wall of sella) (d).  
 Type 4B **Postsellar** (posterior wall of sphenoid sinus is behind the posterior wall of sella, with air dorsal to the sella) (e).

### Coronal Plane

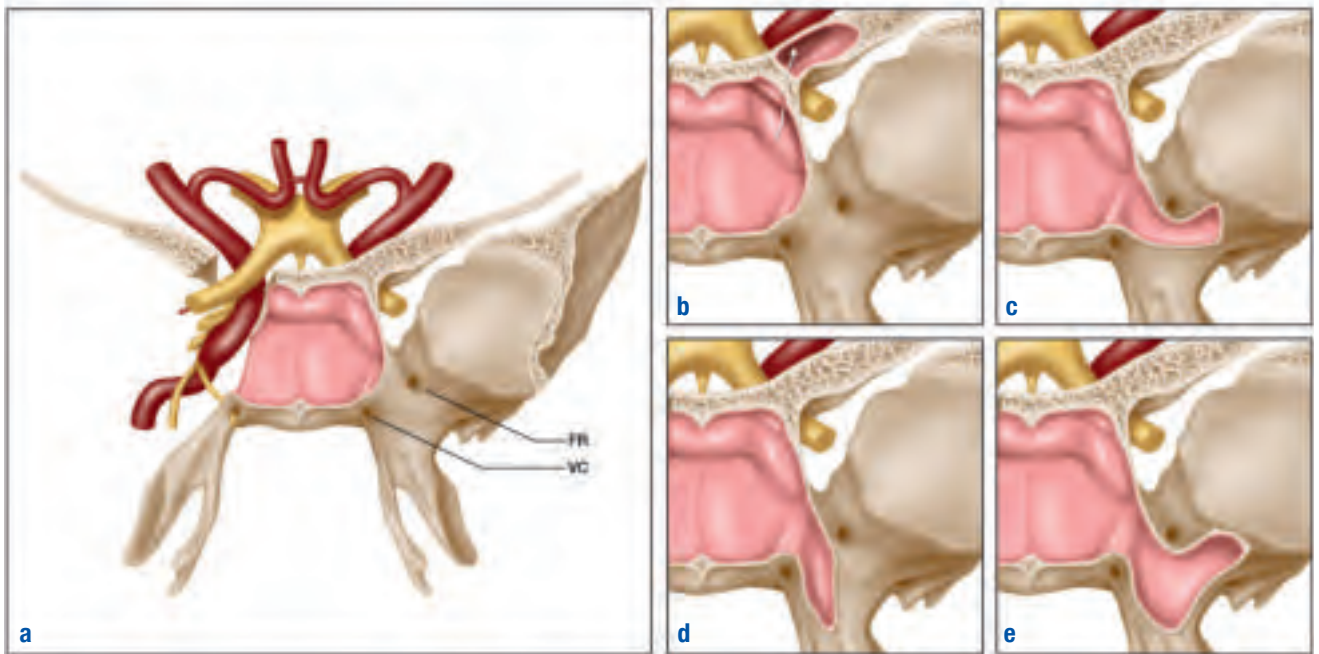


**Fig. 2.5**

- Body Type** – The pneumatization is confined to the body of the sphenoid sinus (a).  
**Lesser Wing Type** – The sinus pneumatizes through the optic strut (arrow) and into the anterior clinoid process (b).  
**Greater Wing Type** – The pneumatization extends laterally between the foramen rotundum (FR) and vidian canal (VC) into the greater wing (c).  
**Pterygoid Type** – The pneumatization extends laterally between the FR and VC and inferiorly into the pterygoid process (d).  
**Full Lateral Type** – The sinus extends laterally into both the greater wing and the pterygoid process (e).

## Age-Dependent Sphenoid Pneumatization Patterns

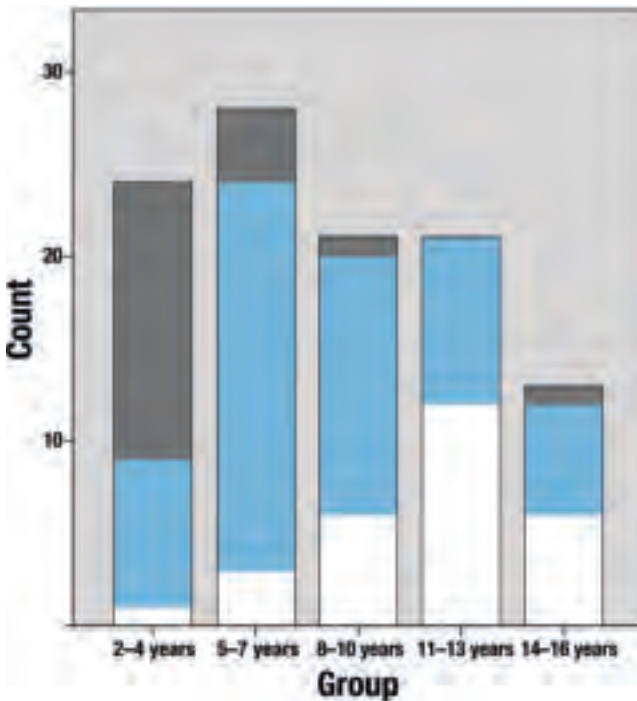


**Fig. 2.6** Bar graphs showing sphenoid pneumatization pattern (conchal, presellar, sellar) in the pediatric population by age group. With increasing age, the sellar and presellar pneumatization patterns are most commonly encountered. Conchal (dark grey), Presellar (blue), Sellar (white).

Pneumatization patterns are a relative limitation in pediatric endoscopic endonasal surgery because the cancellous bone can be easily drilled down to approach the sella, as seen in [Fig. 2.7](#).

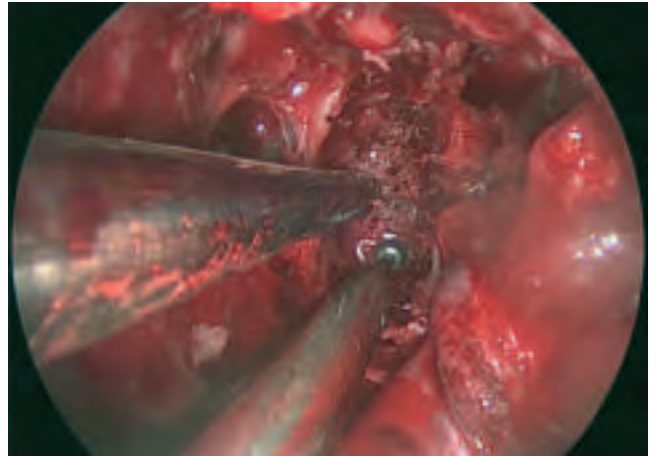


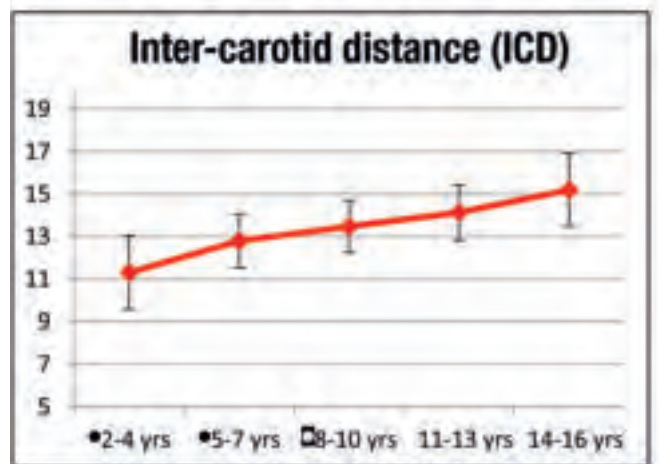
**Fig. 2.7**

## 2.4 Inter-Carotid Distance (ICD)

The inter-carotid distance (ICD), measured in millimeters, at the cavernous sinus imposes absolute limitations to pediatric endoscopic endonasal approaches, and is directly affected by the pneumatization process. The ICD increases with age, as shown in the graph below.

According to our experience, while patient age and size is not a significant limitation to the endoscopic endonasal approach, a wider inter-carotid distance (ICD) and shorter dens-nare distance predicts better outcomes and fewer complications.

**Fig. 2.8** The graph demonstrates how the inter-carotid distance (ICD) grows with age.



## 2.5 Pediatric Naso-Septal Flap Harvest

While harvesting the naso-septal flap (NSF) in the pediatric population, care must be taken to preserve the olfactory epithelium (OE) above and the maxillary crest growth plate (MCGP) below.

The mucosal flap from the contralateral side can be swung over to cover the denuded septum (S), thereby preserving nasal function and reducing sinonasal complications.

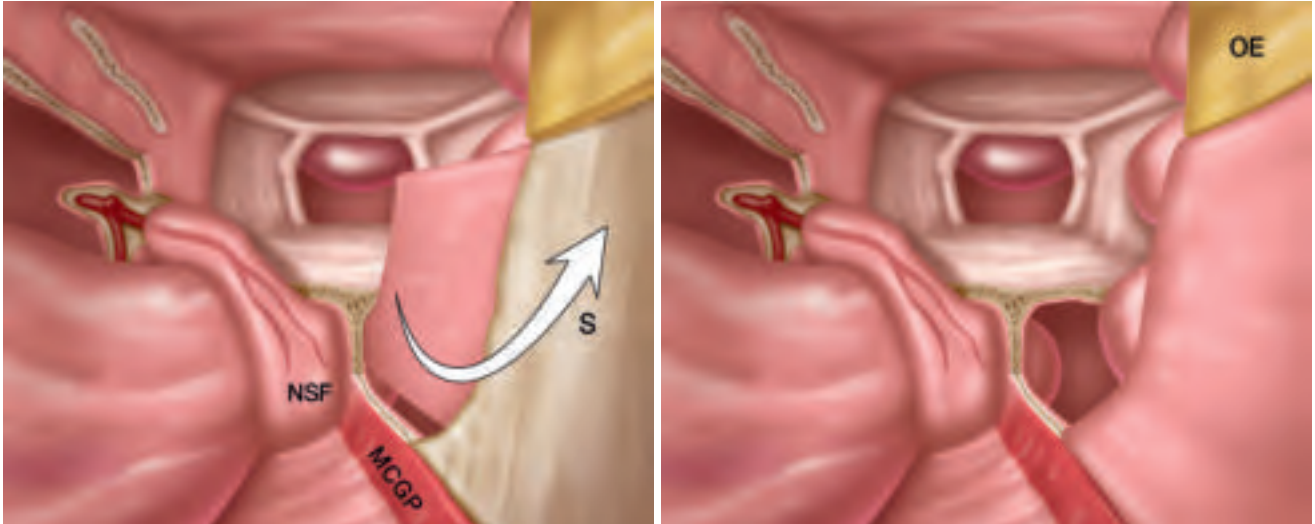


**Fig. 2.9** Naso-septal flap harvest.

Naso-septal flap (NSF); olfactory epithelium (OE); maxillary crest growth plate (MCGP); septum (S).

# 3

## Pathology Unique to the Pediatric Skull Base

Some of the more frequent pediatric lesions occurring in the suprasellar region are as follows: craniopharyngioma, chiasmatic glioma, germ cell tumor, juvenile angiofibroma and basilar invagination/platybasia.

### 3.1 Craniopharyngioma

Craniopharyngiomas account for between 1% and 4% of all pediatric brain tumors and are the most commonly diagnosed tumors of the sellar and suprasellar region in children. Pediatric craniopharyngioma, representing 30–50% of all cases of craniopharyngioma, is almost exclusively of the adamantinomatous subtype with a Beta-catenin mutation rather than the papillary subtype, which is more commonly found in adults. Involvement of the

hypothalamus is common in pediatric craniopharyngiomas (> 90%) at the time of diagnosis, posing a significant challenge to surgical resection and long-term quality of life. Avoiding damage to the hypothalamus is critical to avoid cognitive decline and obesity and subtotal resection may be preferable in certain cases to avoid these complications.

### 3.2 Chiasmatic Glioma

Optic pathway gliomas, of which chiasmatic gliomas are a subset, account for 2–5% of childhood brain tumors and are typically found at approximately 4–5 years of age. Optic pathway gliomas are frequently detected in children with neurofibromatosis 1 (NF1); however, most chiasmatic gliomas occur in children without NF1.

Chiasmatic gliomas are frequently complicated by involvement of the hypothalamus and third ventricle, which in a fashion similar to craniopharyngioma can cause hydrocephalus.

### 3.3 Germ Cell Tumors

Germ cell tumors (GCTs), including germinomas, non-germinomatous GCTs (NGGCTs), and teratomas, account for approximately 3% of primary pediatric brain tumors. The suprasellar region is one of the two most common regions for GCTs, the other being the pineal region. Common presenting features of germ cell tumors in the suprasellar

region include diabetes insipidus, visual field defects, and hypothalamic-pituitary dysfunction. Radiation therapy is extremely effective in treating germinomas, and complete responses are often achieved with craniospinal radiation alone. Biopsy is sometimes necessary to make a pathologic diagnosis.

### 3.4 Juvenile Angiofibroma

Juvenile angiofibroma (JNA) is a benign vascular lesion that occurs in the nasopharynx of prepubertal and adolescent males. Juvenile nasopharyngeal angiofibroma (JNA) accounts for 0.05% of all head and neck tumors, and occurs exclusively in males. Onset is most com-

monly in the second decade (7–19 years). The lesion originates in close proximity to the posterior attachment of the middle turbinate, near the superior border of the sphenopalatine foramen.

### 3.5 Basilar Invagination/Platybasia

Basilar invagination is a congenital or acquired craniocervical junction abnormality where the tip of the odontoid process projects above the foramen magnum. It may be congenital or acquired and is often associated with platybasia: stenosis of the foramen magnum and compres-

sion of the medulla oblongata. If the condition develops after birth, it is usually the result of injury or diseases. It is associated with bone diseases such as osteomalacia, rheumatoid arthritis, Paget's disease, Ehlers-Danlos syndrome, Marfan syndrome, and osteogenesis imperfecta.

# 4

## Operating Room Set-Up

### 4.1 Endonasal Approach with Intraoperative Image Guidance Using Preoperative Magnetic Resonance Imaging (MRI)

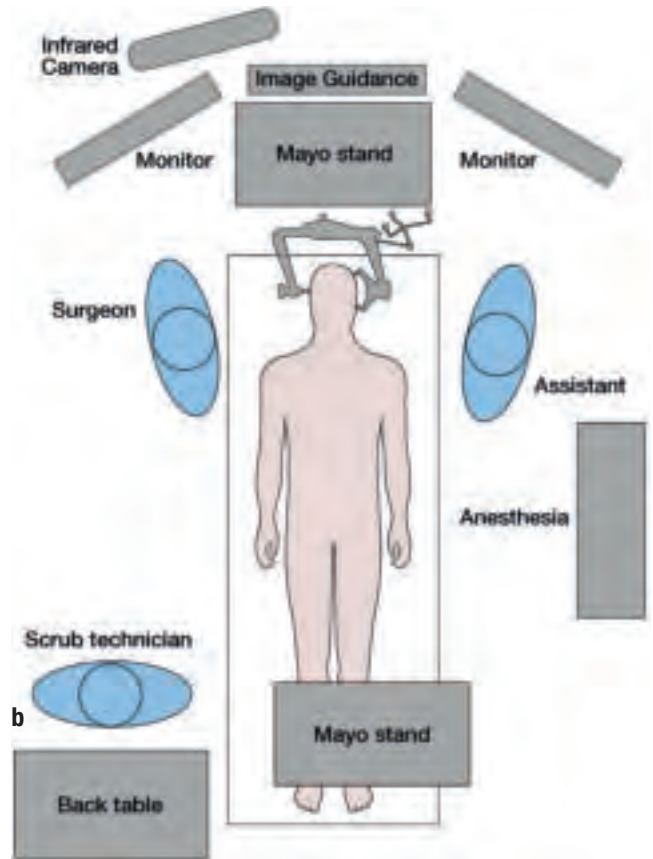


**Fig. 4.1** Intraoperative situation during an endonasal approach with intraoperative image guidance using preoperative magnetic resonance imaging (MRI) (a) and schematic bird's eye view of the operating room set-up (b).

### 4.2 Endonasal Approach with Image Guidance Using Live Intraoperative Computed Tomography (CT)

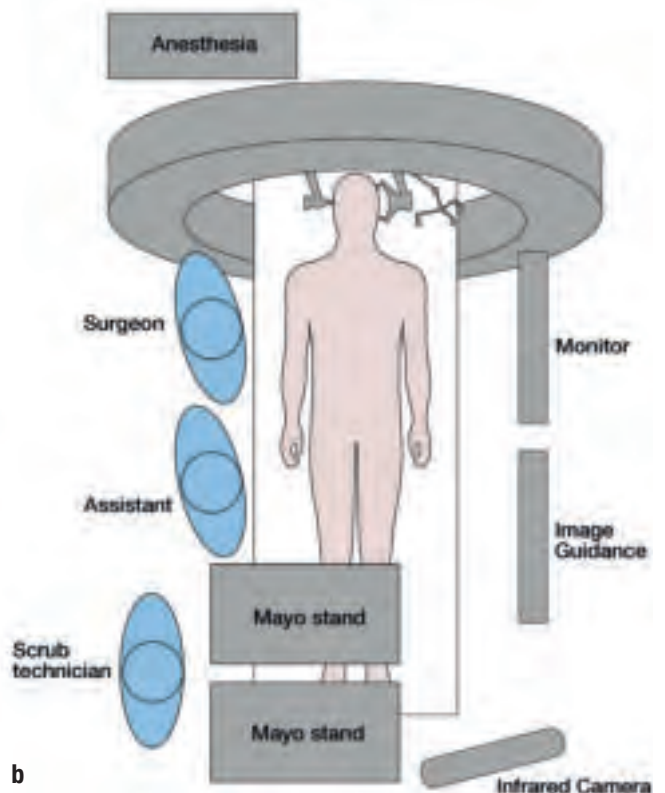


**Fig. 4.2** Intraoperative situation during an endonasal approach with image guidance using live intraoperative computed tomography imaging (CT) (a) and schematic bird's eye view of the operating room set-up (b).

## 5

## Endonasal Corridors and Approaches

### 5.1 Transnasal and Transfrontal

The transnasal corridor does not involve any breach of the paranasal sinuses. Approaches to the cribriform plate, the inferior 2/3rd of the clivus and odontoid are feasible through this surgical corridor. The frontal sinus can be reached via the transfrontal approach.

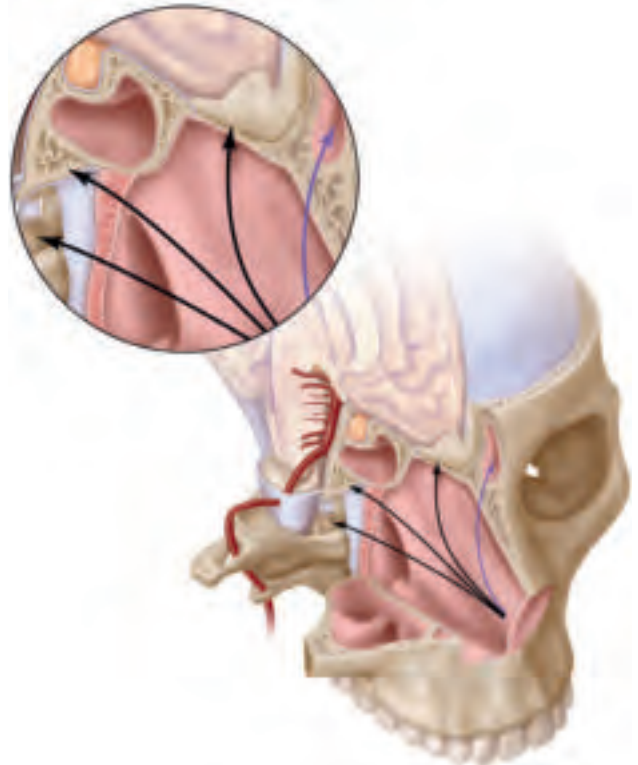


**Fig. 5.1** Schematic drawing showing the transnasal (→) and transfrontal (→) corridors.

### 5.2 Transsphenoidal

The transsphenoidal corridor is the most commonly used corridor and permits approaches to the sella, suprasellar cistern, medial cavernous sinus and superior clivus.

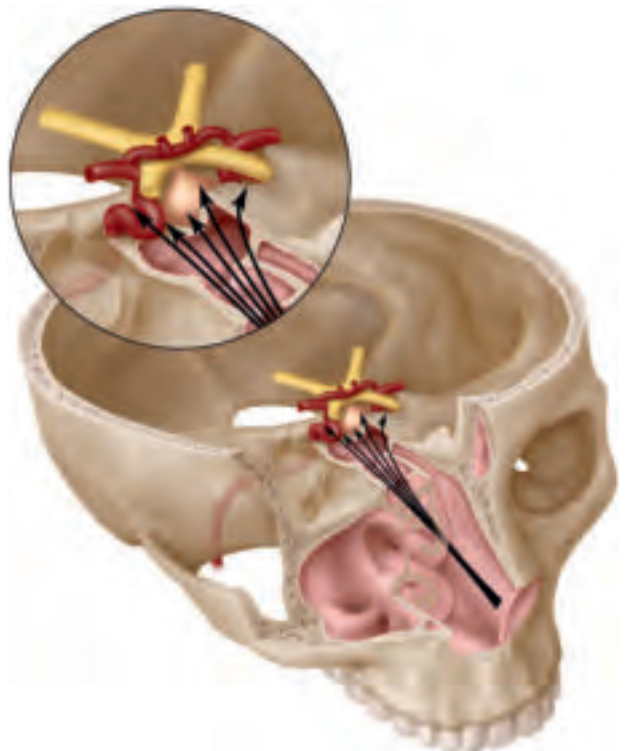


**Fig. 5.2** Schematic drawing showing the transsphenoidal (→) corridor.

### 5.3 Transethmoidal

The transethmoidal corridor exposes the orbital apex, the lateral cavernous sinus, and the anterior fossa through the fovea ethmoidalis.

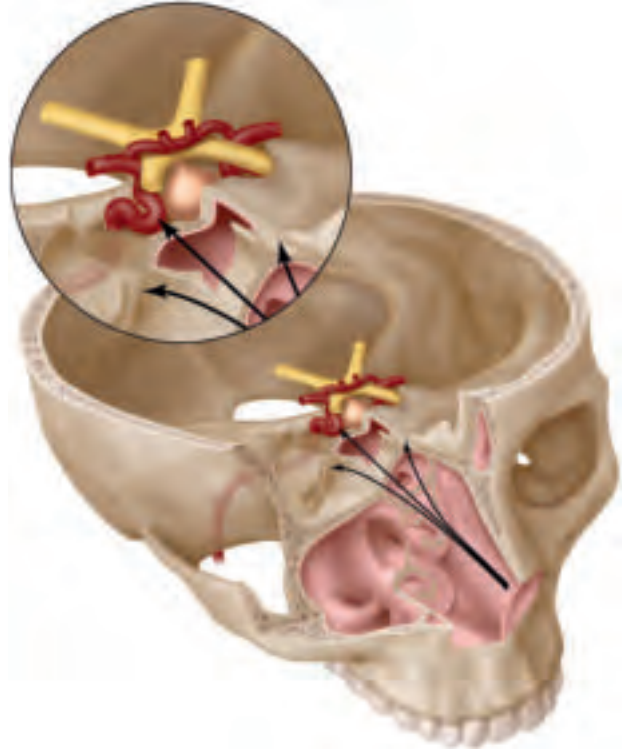


**Fig. 5.3** Schematic drawing showing the transethmoidal (→) corridor.

### 5.4 Transmaxillary

The transmaxillary corridor facilitates approaches to the pterygopalatine fossa, the petrous apex, Meckel cave, and the infratemporal fossa.

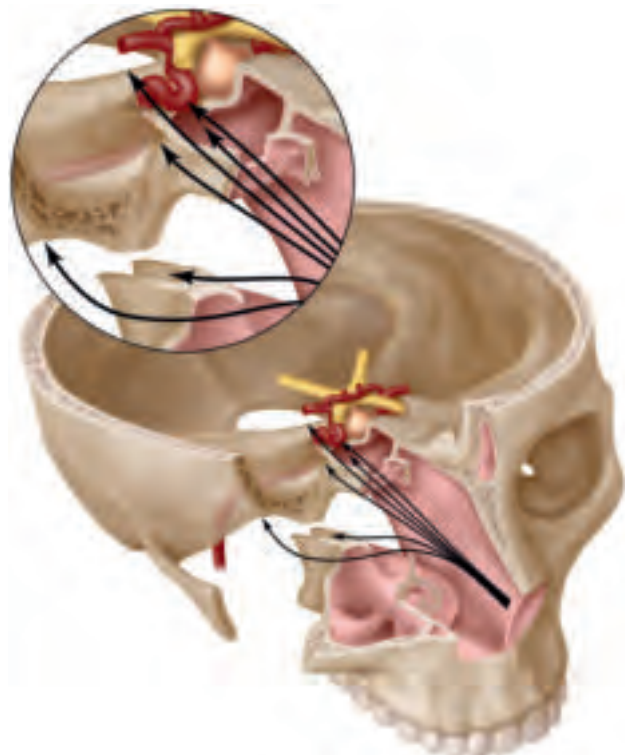


**Fig. 5.4** Schematic drawing showing the transmaxillary (→) corridor.

## 6

## Surgical Approaches – Clinical Cases and Operative Images

### 6.1 Transtuberculum Approach for Craniopharyngioma

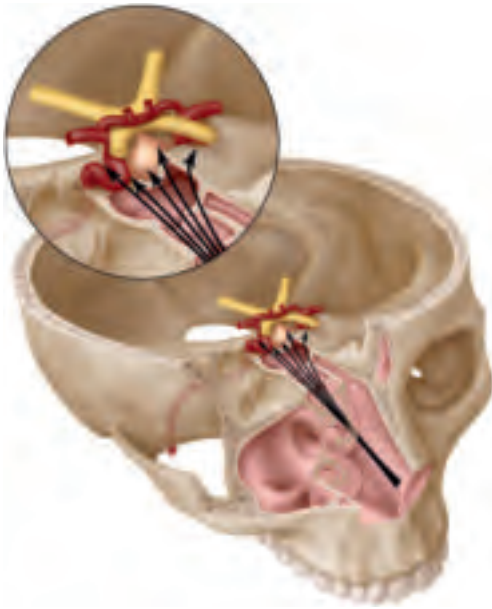


**Fig. 6.1** Transtuberculum approach using the transphenoidal corridor.

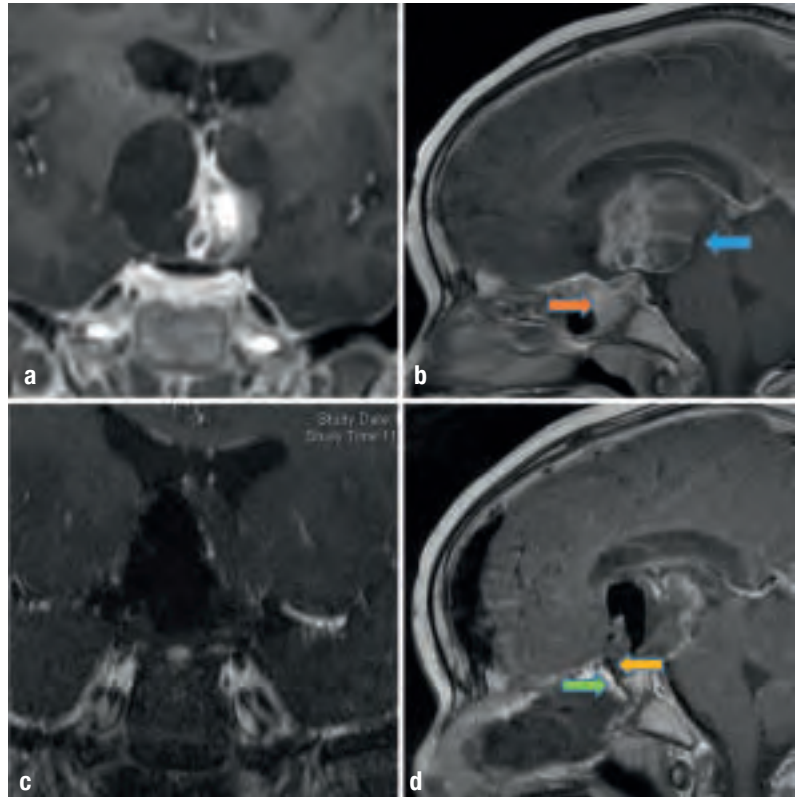


**Fig. 6.2** Preoperative coronal and sagittal T1-weighted MRI images (a, b) showing an enhancing cystic suprasellar lesion with extension into the third ventricle and adherence to the hypothalamus (←). Note the conchal pattern of pneumatization of the sphenoid (→). Postoperative imaging (c, d) showing intended sub-total resection (STR) of lesion (→). The MEDPOR graft used for skull base reconstruction can be visualized (→), as well as the naso-septal flap (→).

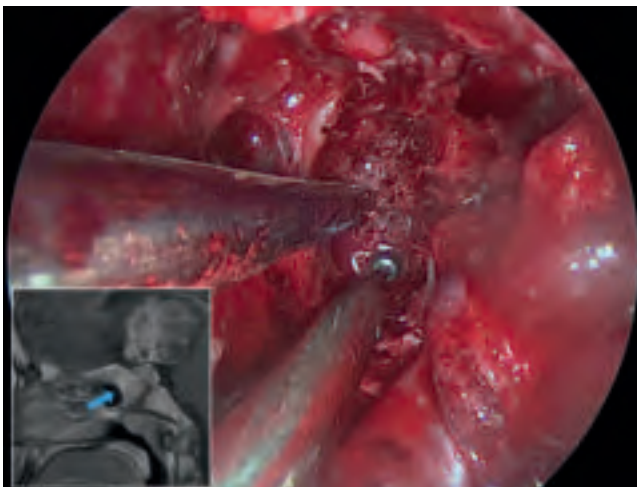


**Fig. 6.3** Incomplete pneumatization (Conchal type) of the sphenoid is seen (←). The cancellous bone can be easily drilled to reach the sella.

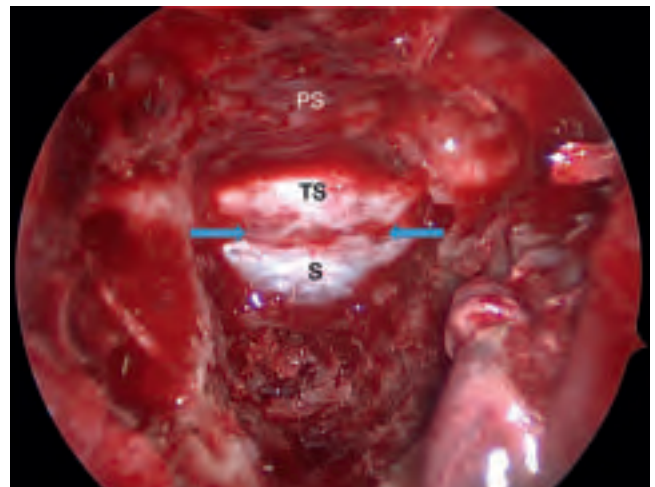


**Fig. 6.4** The dura over the sella (S), tuberculum sella (TS) and planum sphenoidale (PS) is exposed. The intercavernous sinus is visualized (←).

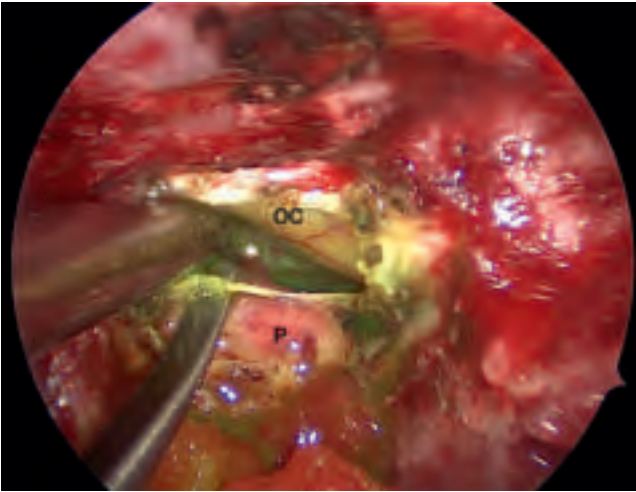


**Fig. 6.5** The dura is opened above and below the intercavernous sinus, over the sella and the tuberculum sella. The optic chiasm (OC) and pituitary gland (P) are visualized. The pituitary stalk (\*) is also seen. The green staining of the CSF is from the fluorescein dye, which was injected via a lumbar puncture prior to the start of the case.

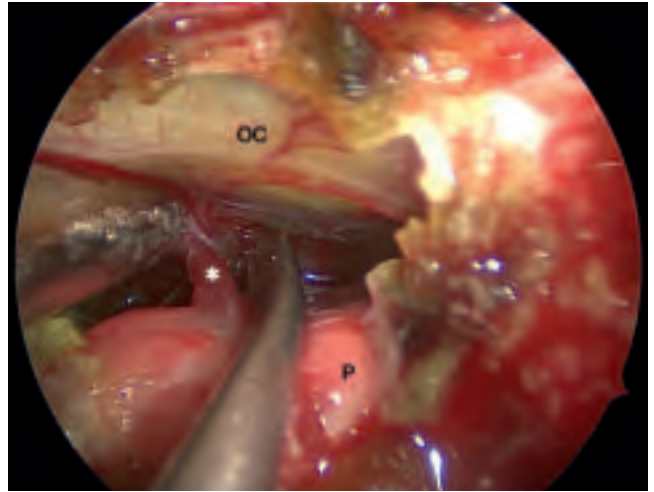


**Fig. 6.6** Mobilizing tumor from the 3<sup>rd</sup> ventricle, posterior to the pituitary stalk (\*).

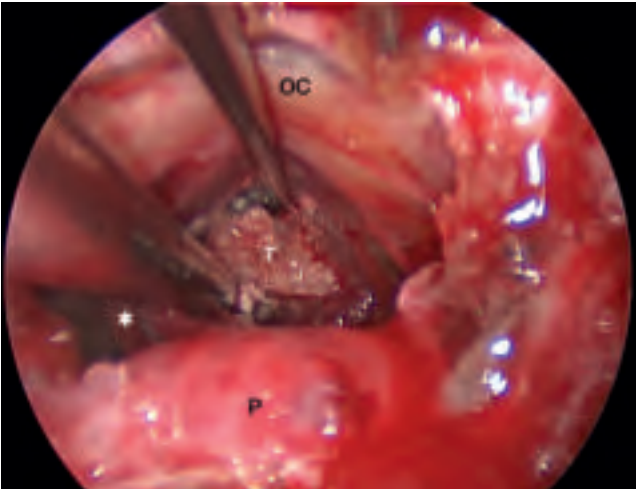


**Fig. 6.7** Resection of tumor (T) in a piecemeal fashion. The pituitary stalk (\*) is indented over the suction.

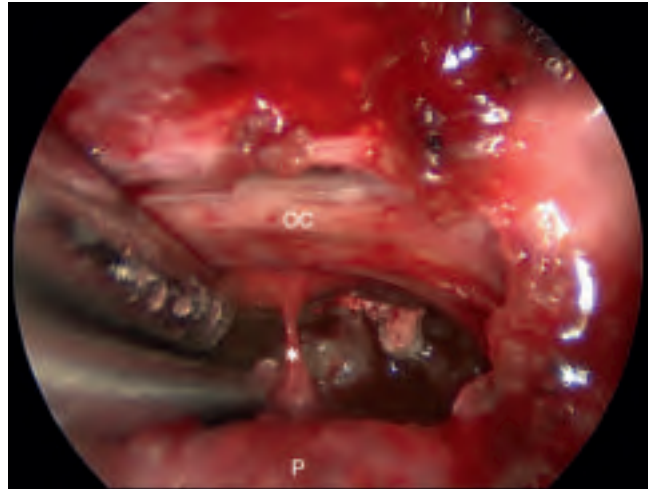


**Fig. 6.8** Removing the last few fragments of tumor. The thinned out pituitary stalk (\*) is seen. Small fragments of the capsule are stuck to the hypothalamus and are left behind. Closure is performed with fascia lata and MEDPOR gasket seal layered with a pedicled naso-septal flap. This technique is illustrated in a later section of this manual. Optic chiasm (OC); pituitary gland (P).

## 6.2 Transplanum Approach for Juvenile Pilocytic Astrocytoma (JPA)



**Fig. 6.9** Transplanum approach using the transsphenoidal corridor.

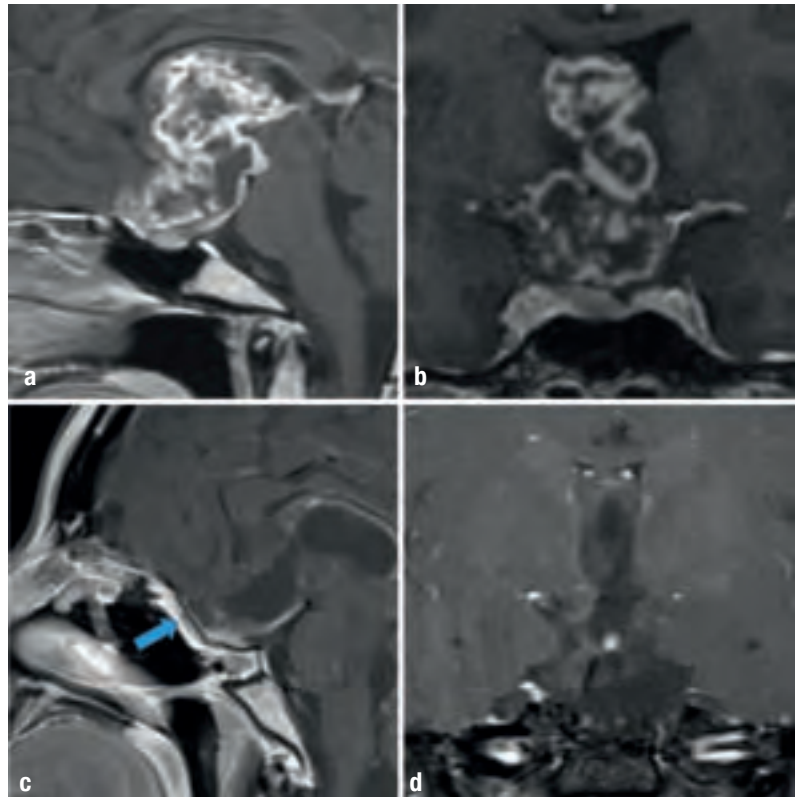


**Fig. 6.10** Preoperative (a, b) sagittal and coronal MRI images (T1 weighted with Gadolinium) showing the Juvenile Pilocytic Astrocytoma (JPA). Postoperative images (c, d) showing gross total resection of the JPA. Placement of the MEDPOR graft (←) to reconstruct the skull base post resection.

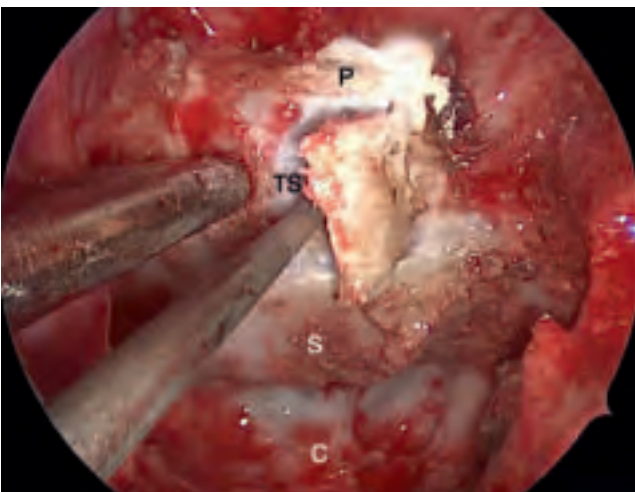


**Fig. 6.11** The bone overlying the tuberculum sellae (TS) and planum (P) is drilled and removed. Sella (S); clivus (C).

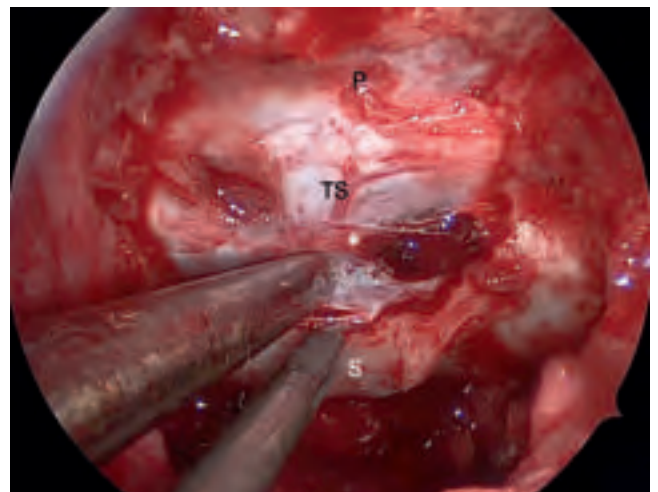


**Fig. 6.12** The dura is sharply incised above and below the intercavernous sinus (\*), and the sinus coagulated and incised.

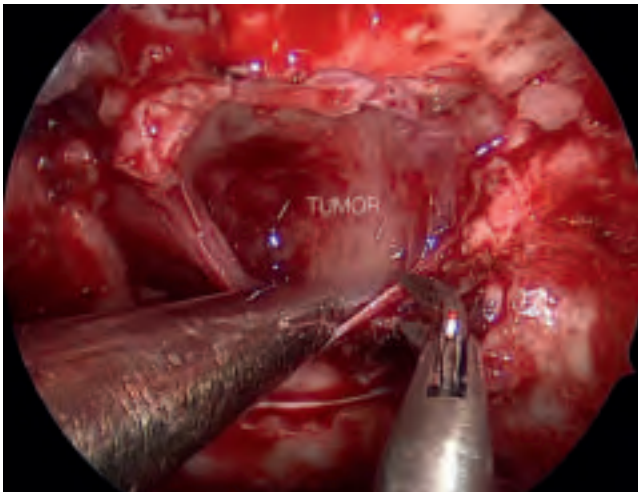


**Fig. 6.13** The tumor capsule is opened leading us into the tumor.

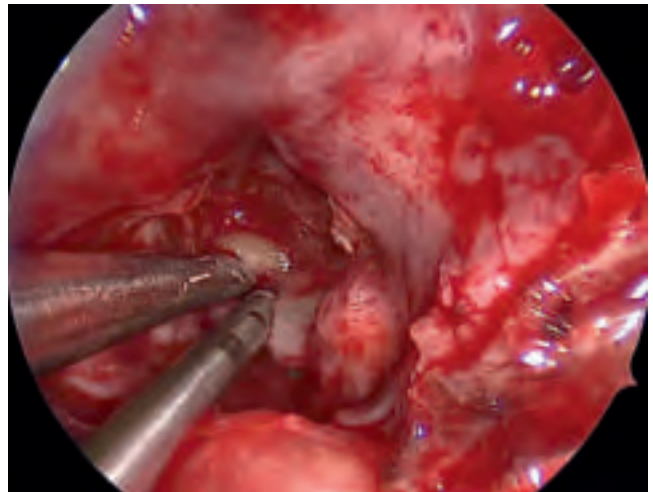


**Fig. 6.14** The tumor is internally debulked using suction and the Nico Myriad device (Nico Corp., Indianapolis, USA).

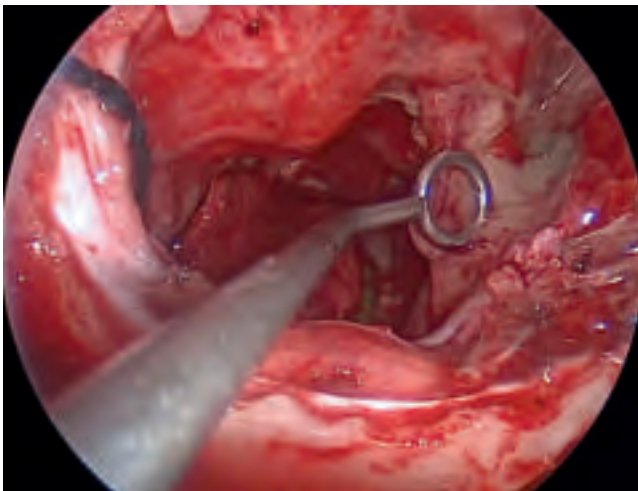


**Fig. 6.15** Once sufficient debulking has been done, the tumor capsule is dissected off the surrounding brain and resected.

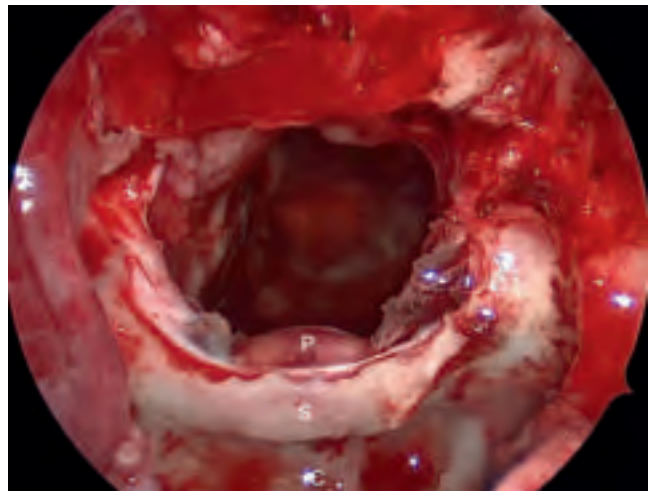


**Fig. 6.16** The tumor cavity post resection. The pituitary gland (P) can be seen inside the sella (S). The skull base is reconstructed using the Gasket technique with MEDPOR and fascia lata, followed by a naso-septal flap. The Gasket technique is illustrated later in this manual.

### 6.3 Transcavernous Approach for Dermoid

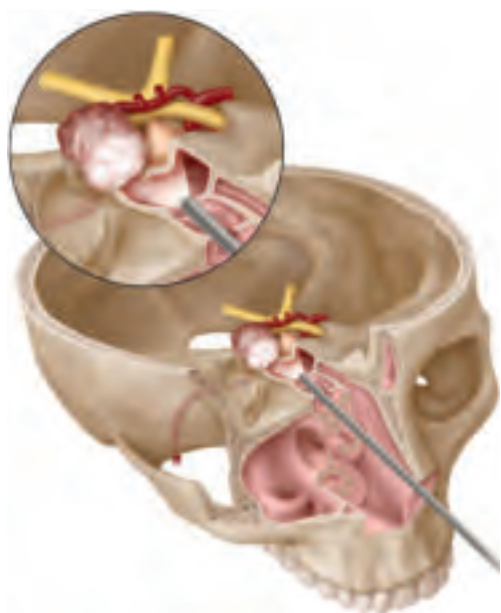


**Fig. 6.17** Transcavernous approach using the trans-sphenoidal corridor.

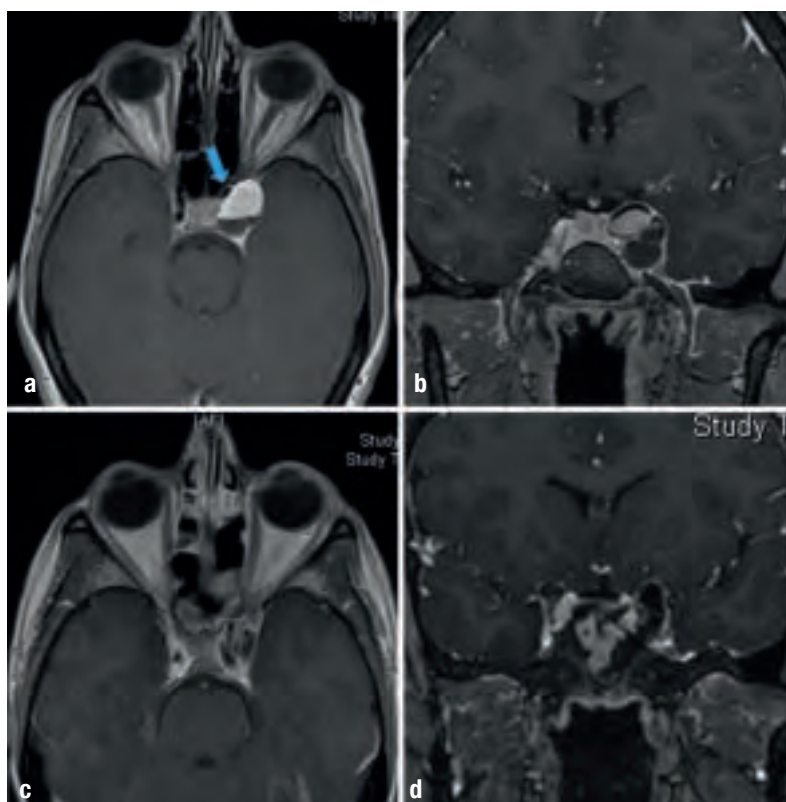


**Fig. 6.18** Preoperative (a, b) and postoperative (c, d) axial and coronal contrast-enhanced T1-weighted MRI sequences, showing a cystic nodular lesion in the left cavernous sinus. The carotid artery is medially displaced by the tumor in the cavernous sinus (←).

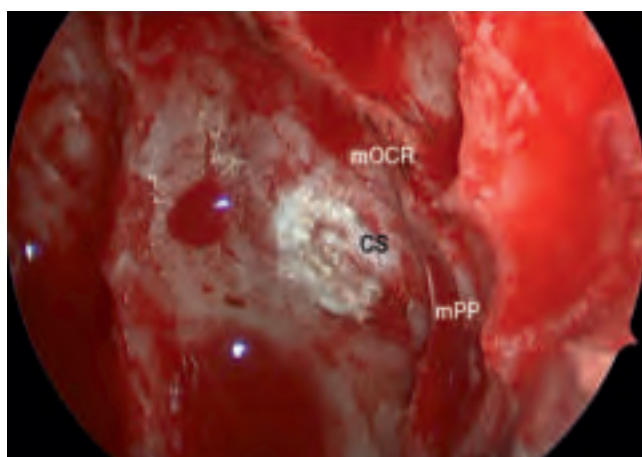


**Fig. 6.19** The bone between the optic nerve and the carotid artery, or medial opticocarotid recess (mOCR) can be removed to expose the superomedial aspect of the cavernous sinus (CS). This opening can be extended inferolaterally to expose the carotid siphon in the medial cavernous sinus. The lateral portion of the cavernous sinus can be explored by removing the medial pterygoid plate (mPP).



**Fig. 6.20** The bone over the medial cavernous sinus is removed. The anterior wall of the pterygopalatine fossa (PF) is removed to reveal the contents. The PF contents are moved laterally to drill the medial pterygoid plate (mPP) to access the lateral portion of the cavernous sinus. The sphenopalatine artery needs to be coagulated and cut (\*) to laterally mobilize the contents of the PF.

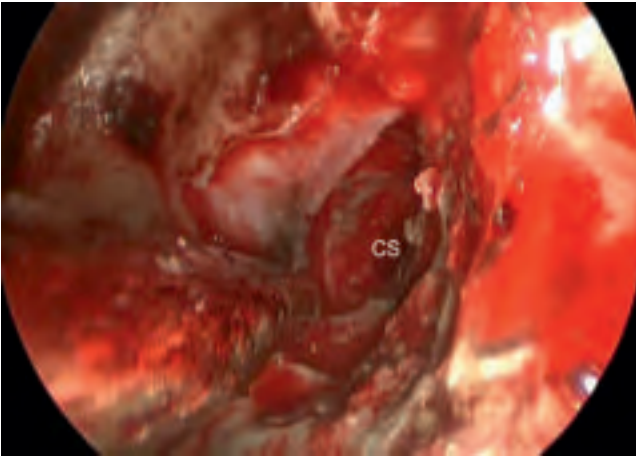


**Fig. 6.21** The medial pterygoid plate is removed. The cavernous sinus (CS) dura is opened sharply with a sickle blade and the opening extended with angled scissors.

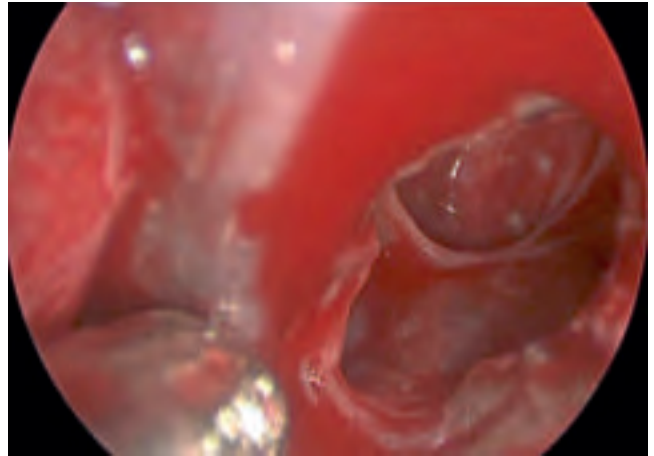


**Fig. 6.22** One can see the septations of the tumor capsule within the cavernous sinus.

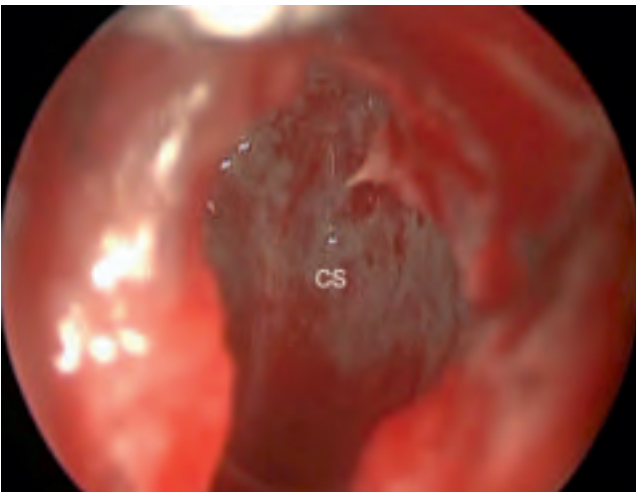


**Fig. 6.23** The posterior wall of the cavernous sinus is visualized after resection of the tumor. Cavernous sinus bleeding is controlled with Floseal and Gelfoam.



**Fig. 6.24** View of the sphenoid (S) sinus after left cavernous sinus tumor resection. The medial pterygoid plate (mPP) on the left has been resected. If there is no CSF leak, closure is achieved with a few small pieces of gelfoam placed in the cavernous sinus (CS).

## 6.4 Transcribriform Approach for Meningoencephalocele



**Fig. 6.25** Transcribriform approach using the trans-nasal corridor.

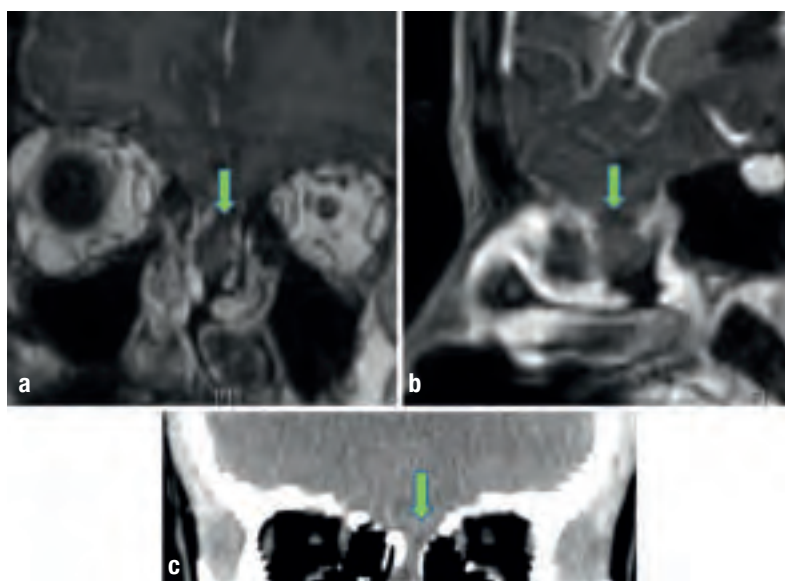


**Fig. 6.26** MRI and CT images showing a soft tissue mass in left superior nasal cavity with associated defect in the left side of the cribriform plate consistent with encephalocele. Cribriform plate defect (→).

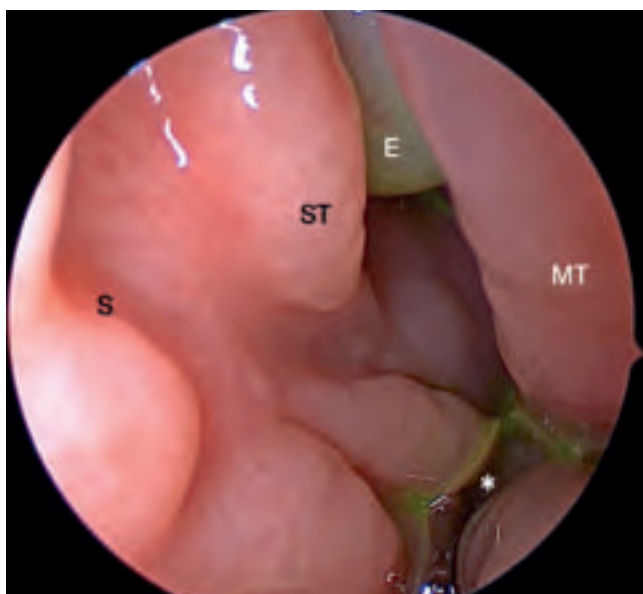


**Fig. 6.27** The encephalocele (E) can be seen between the superior (ST) and middle turbinate (MT) in the left nasal cavity. CSF (\*) tinged with green Fluorescein dye can be seen pooling in the nasal cavity inferiorly. Septum (S).

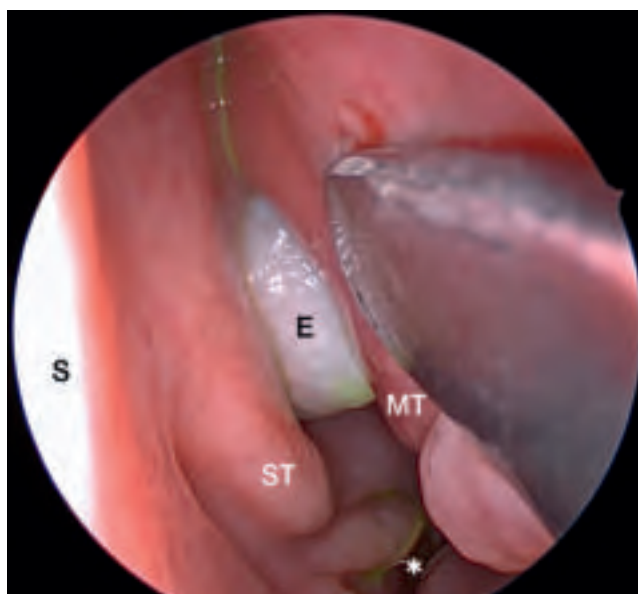


**Fig. 6.28** Another view, looking up from below. The middle turbinate (MT) is displaced laterally by the instrument. CSF (\*) septum (S); superior turbinate (ST); encephalocele (E).

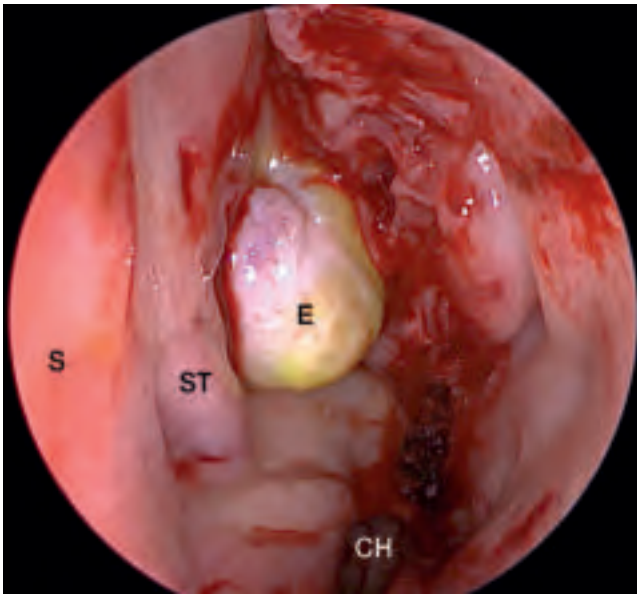


**Fig. 6.29** The middle turbinate is partially resected to fully expose the encephalocele. Choana (CH)

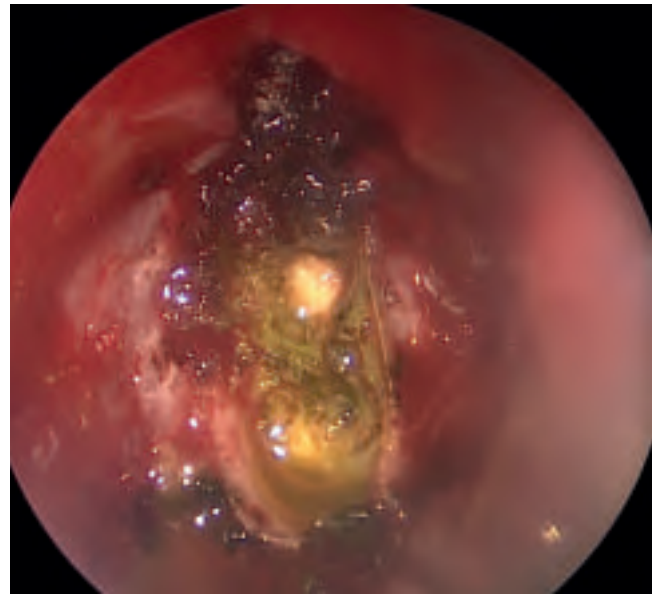


**Fig. 6.30** The encephalocele is resected and the underlying dural and bony defect visualized.

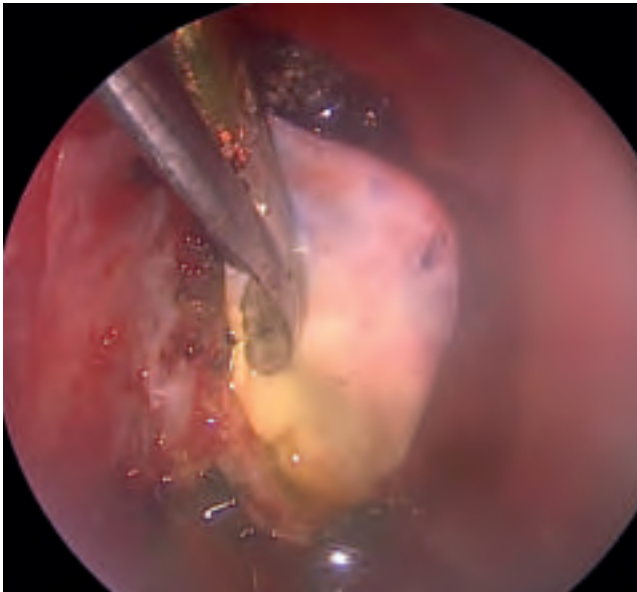


**Fig. 6.31** A small piece of synthetic dura is tucked into the dural defect and used as an inlay graft.

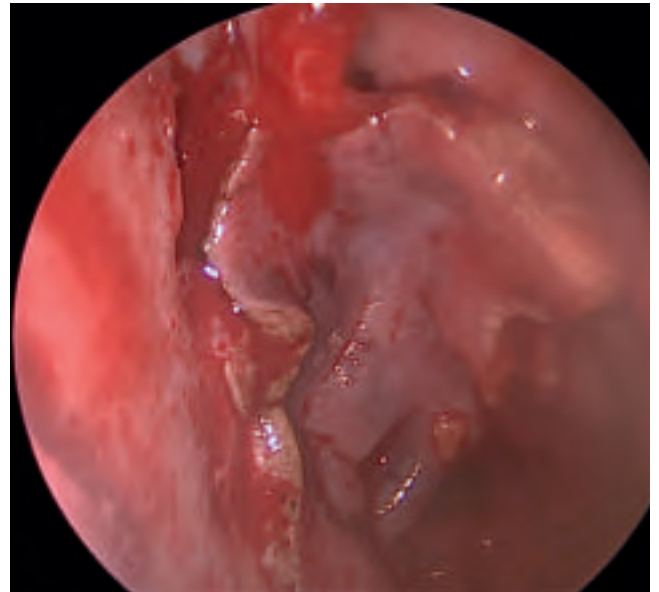


**Fig. 6.32** This is subsequently covered with a small piece of fat followed by the vascularized naso-septal flap to complete the repair.

## 6.5 Transclival Approach for Ependymoma



**Fig. 6.33** Transclival approach using the transnasal corridor.

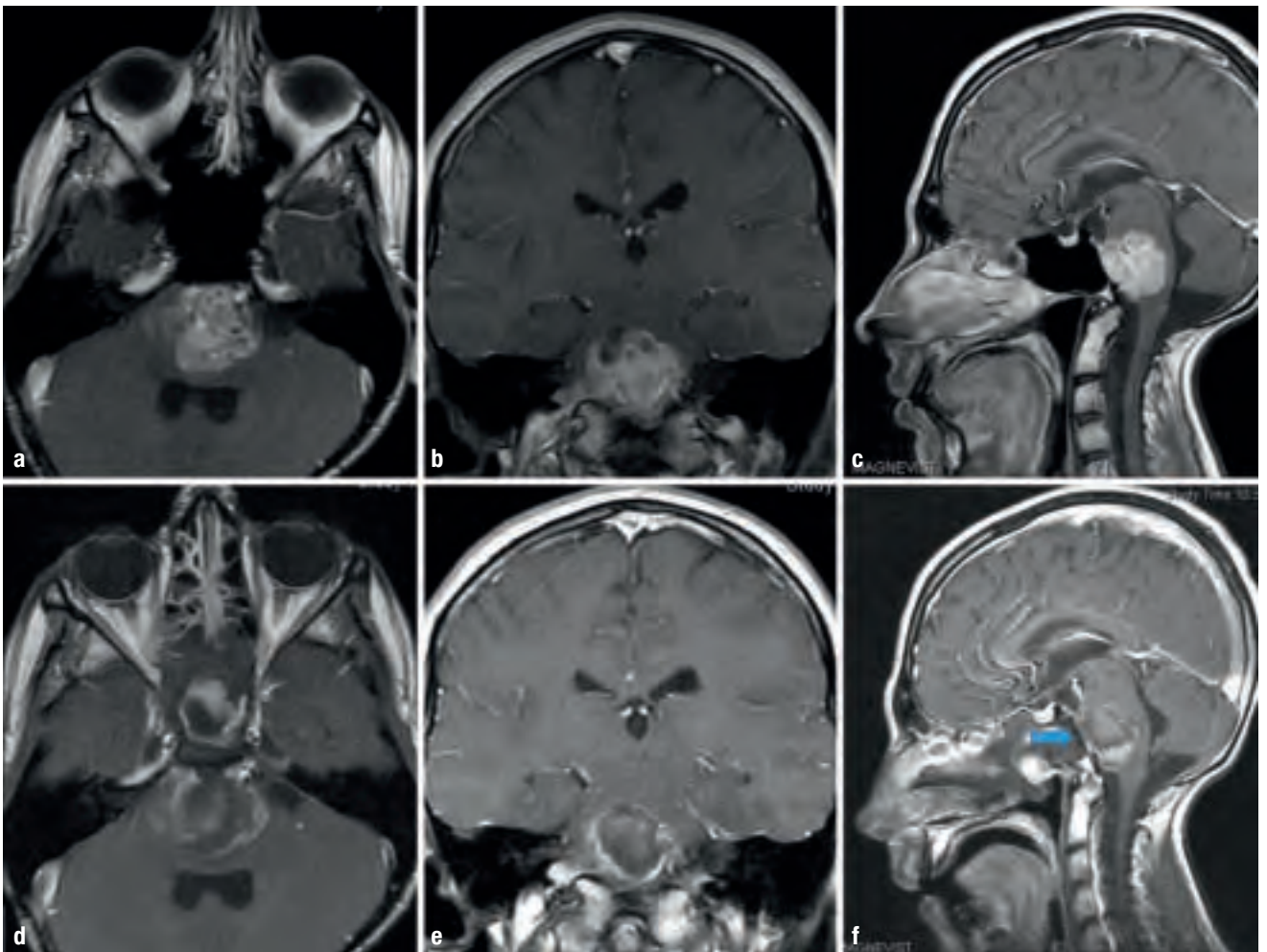


**Fig. 6.34** Preoperative axial (a), coronal (b) and sagittal (c) T1-weighted MRI images showing an enhancing intramedullary lesion in the pons and medulla. Postoperative imaging (d–f) showing sub-total resection (STR) of lesion. The MEDPOR graft used for skull base reconstruction can be visualized (←).

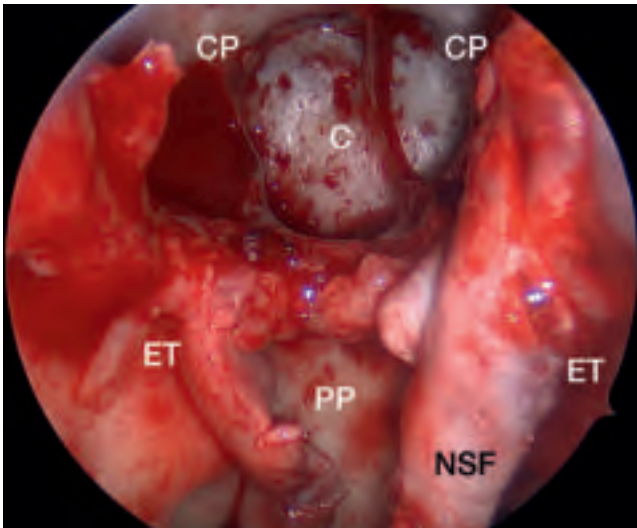


**Fig. 6.35** Transnasal approach to the clivus. The nasoseptal flap (NSF) is harvested and stored in the oropharynx for use in skull base reconstruction. Carotid protuberance (CP); clivus (C); Eustachian tube (ET); posterior pharynx (PP).

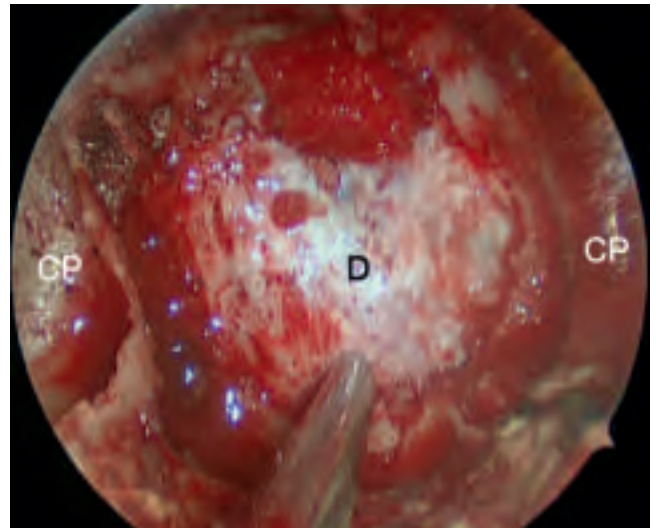


**Fig. 6.36** The clival bone is drilled with a 3-mm round diamond burr and subsequently removed with a 2 mm Kerrison rongeur. The underlying dura (D) is exposed. Carotid protuberance (CP)

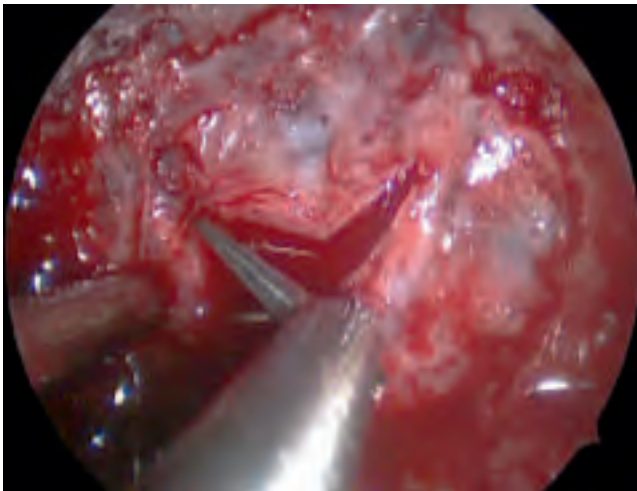


**Fig. 6.37** Stellate opening of clival dura with angled scissors.

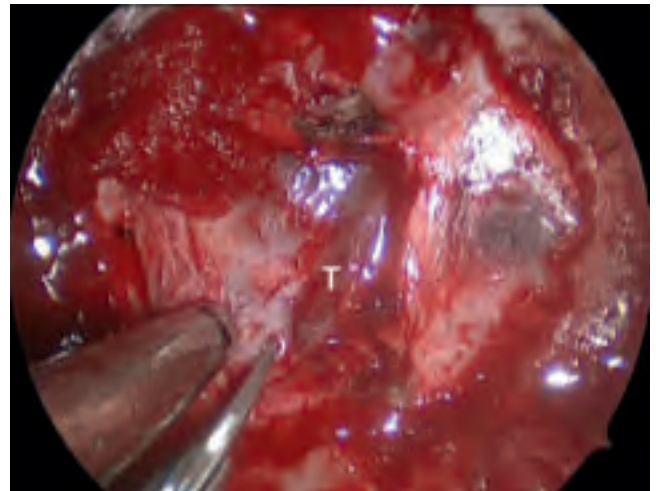


**Fig. 6.38** Intramedullary opening using an 11 blade, revealing grey tumor (T).

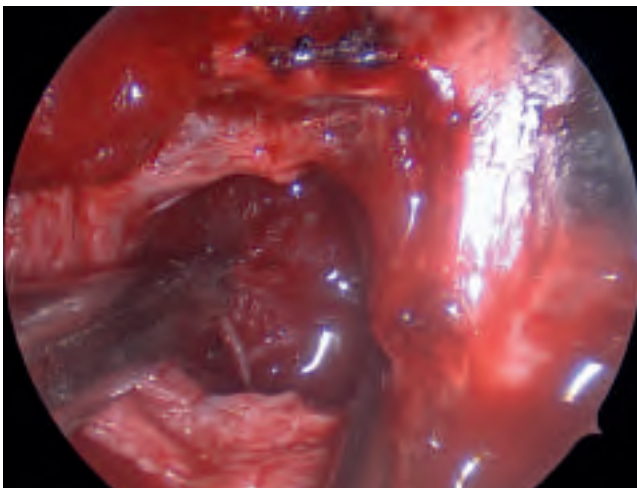


**Fig. 6.39** Intramedullary resection of tumor. Intraoperative neuro-monitoring was used to guide extent of resection during the case.

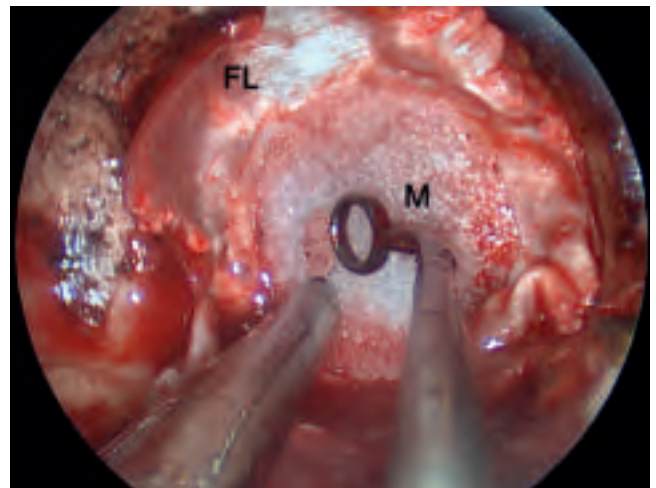


**Fig. 6.40** Gasket seal used for skull base reconstruction, using fascia lata (FL) and MEDPOR (M) graft countersunk into the bony opening. The previously harvested pedicled naso-septal flap was layered over this closure.

## 6.6 Transodontoid Approach for Basilar Invagination

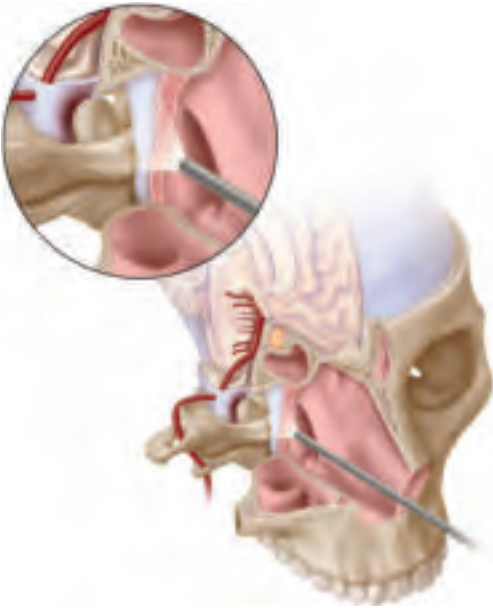


**Fig. 6.41** Transodontoid approach using the transnasal corridor.



**Fig. 6.42** Preoperative (a) T2 weighted sagittal MRI showing basilar invagination with compression of the medulla. Sagittal (b) non-contrast CT prior to the endonasal odontoid resection. Posterior decompression and occiput – C3 fusion is already done for this patient. Sagittal (c) non-contrast CT after endonasal odontoid resection. The cephalad portion of the odontoid, the caudal portion of the clivus and the anterior portion of the C1 ring has been resected.

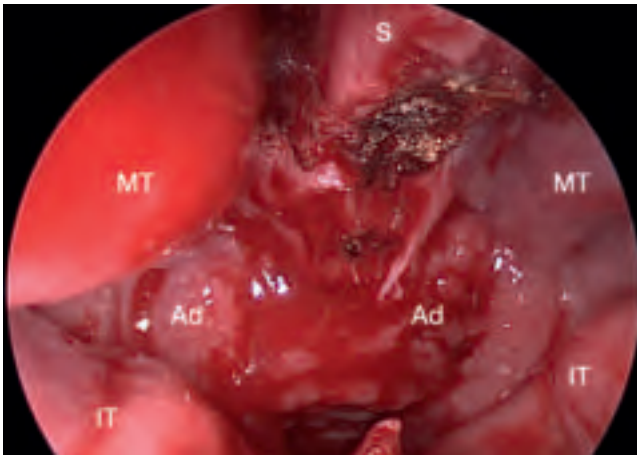


**Fig. 6.43** A posterior septectomy is performed and the nasopharynx approached using a binarial approach. In pediatric patients, large adenoids (**Ad**) can occasionally obscure the choana. Septum (**S**); middle turbinate (**MT**); inferior turbinate (**IT**).

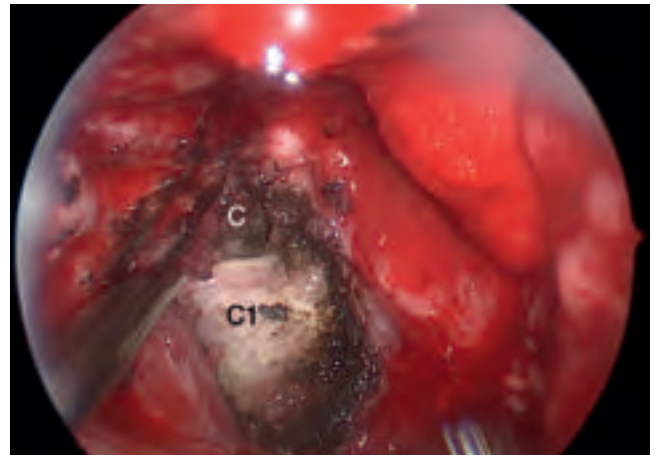


**Fig. 6.44** The adenoids are resected and a vertical incision made in the posterior pharyngeal musculature using bovie electrocautery. The anterior arch of the C1 ring can be seen underneath. The clival mucosa can also be cauterized to expose the clivus (**C**) above. In some cases of severe invagination, the inferior portion of the clivus might also need to be drilled and removed.

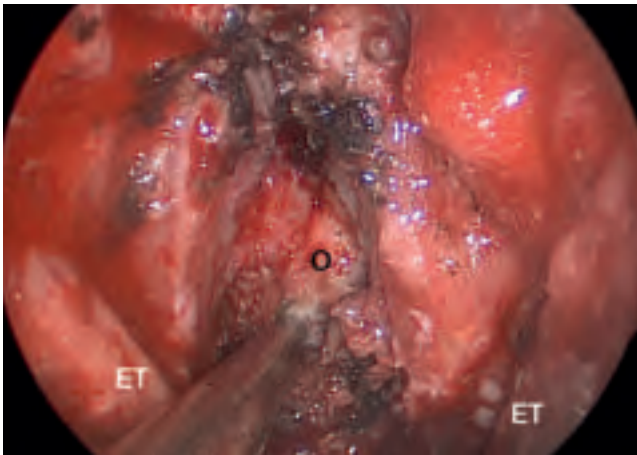


**Fig. 6.45** The anterior arch of C1 is drilled off to expose the odontoid peg. The Eustachian tubes (**ET**) mark the lateral borders of the dissection.

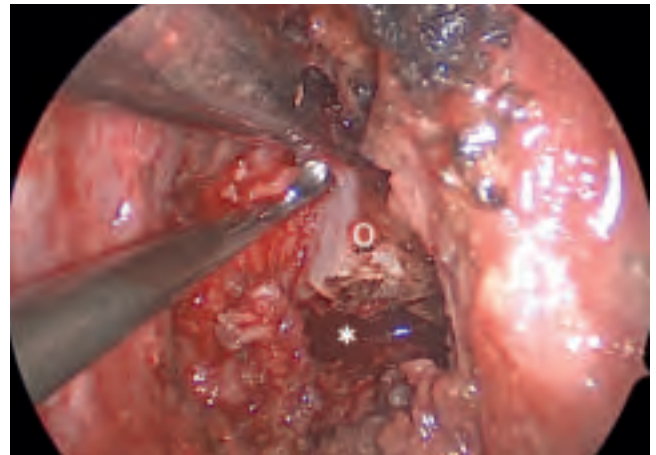


**Fig. 6.46** The odontoid (**O**) peg is hollowed out with a high speed drill and then detached at the base (\*). The remainder of the odontoid shell must be detached from the apical and alar ligaments superiorly and the cruciate ligament posteriorly for complete removal.

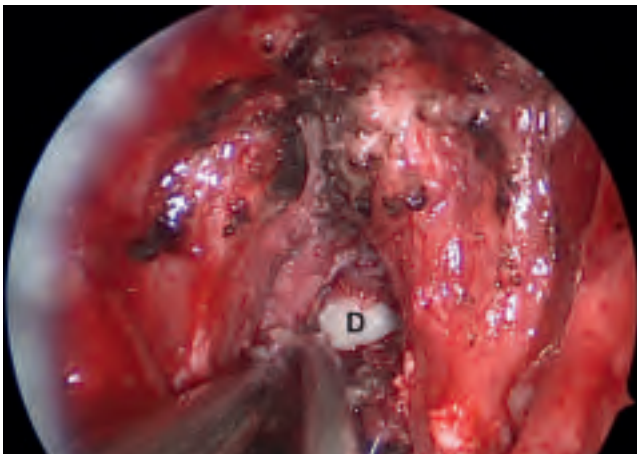


**Fig. 6.47** Once the odontoid peg and cruciate ligament are removed, glistening dura (**D**) can be seen. Care must be taken to not cause a CSF leak while detaching the odontoid and cruciate ligament from the underlying dura.

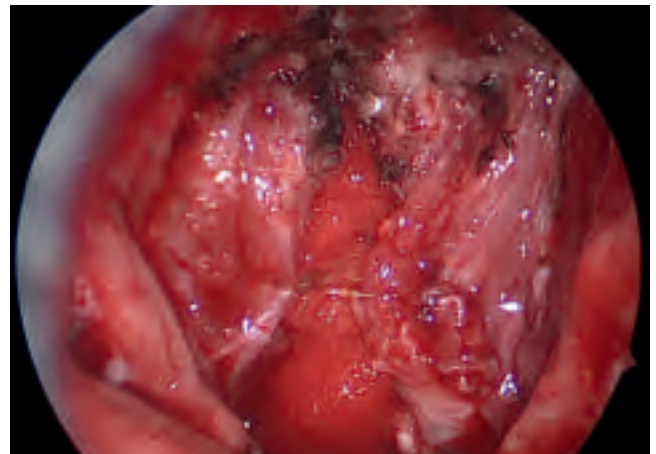


**Fig. 6.48** The posterior pharyngeal musculature is approximated together using absorbable stitches. Gel foam can be placed in the cavity to eliminate the dead space.

## 6.7 Transorbital Approach for Rhabdomyosarcoma



**Fig. 6.49** Transorbital approach using the trans-ethmoidal corridor.

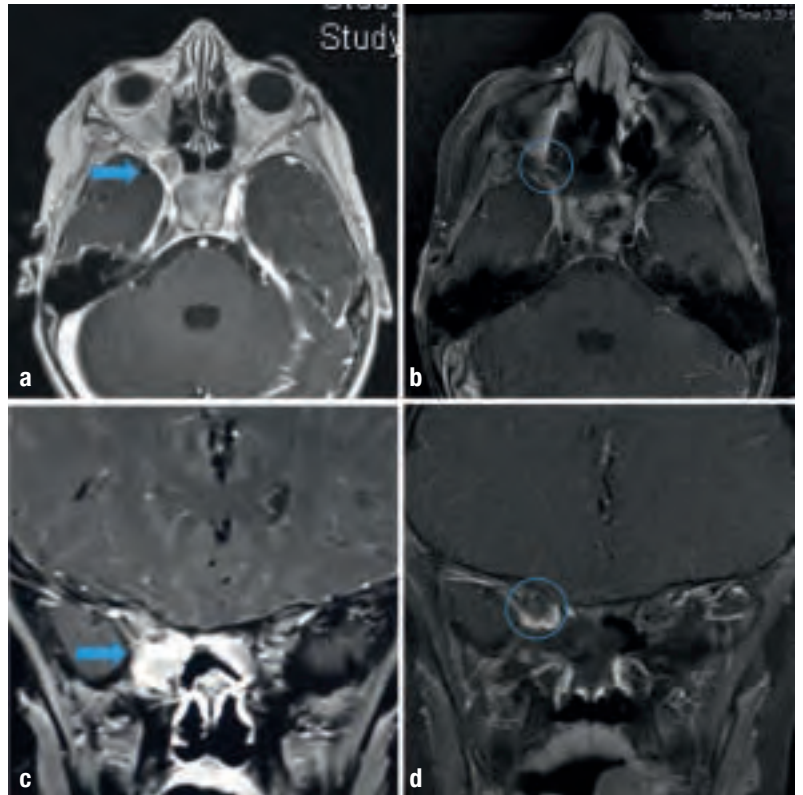


**Fig. 6.50** Note the enhancing lesion (←) at the right orbital apex (a, b). Postoperative axial (c) and coronal (d) MRI sequences with gadolinium enhancement showing resection of tumor.

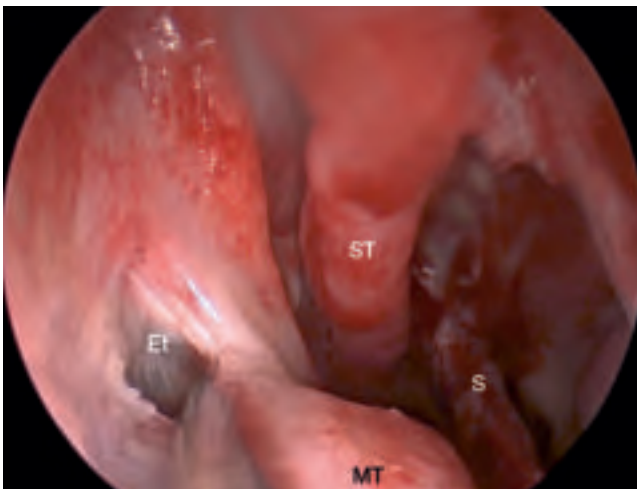


**Fig. 6.51** Right middle meatal exposure: Working lateral to the septum (S) and middle turbinate (MT), the mucosa over the ethmoidal cell (Et) is sharply resected. Note that the posterior septum has been partially resected here to allow for a binarial approach. Superior turbinate (ST).

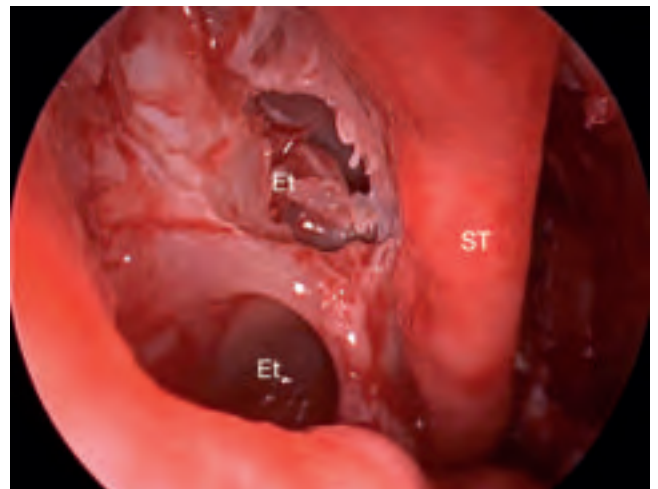


**Fig. 6.52** Complete ethmoidectomy is performed.

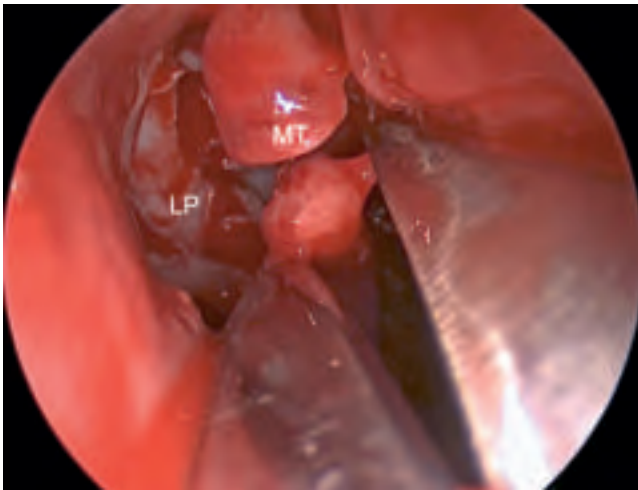


**Fig. 6.53** The inferior portion of the middle turbinate (MT) is incised with scissors and resected, to allow for better visualization of the medial wall of the orbit, the lamina papyracea (LP). The cephalad 3–4 mm of the superior turbinate has high density of olfactory fibers, and is therefore preserved.

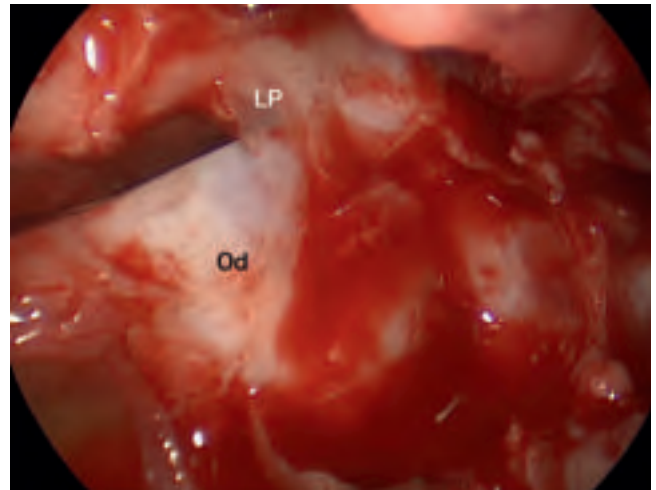


**Fig. 6.54** The lamina papyracea (LP) is removed revealing the medial orbital dura (Od).

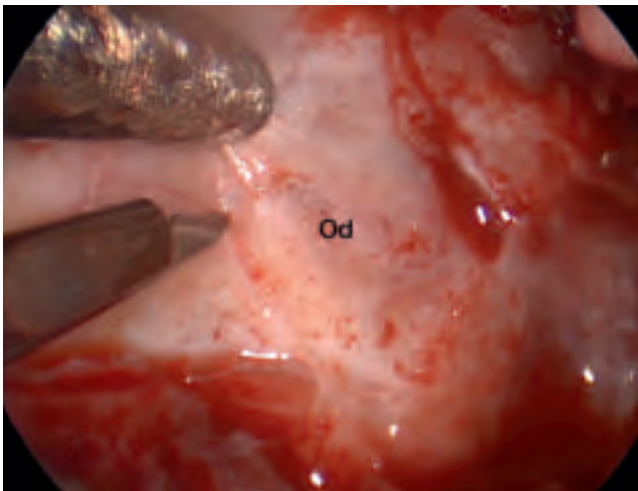


**Fig. 6.55** The medial orbital dura is sharply incised.

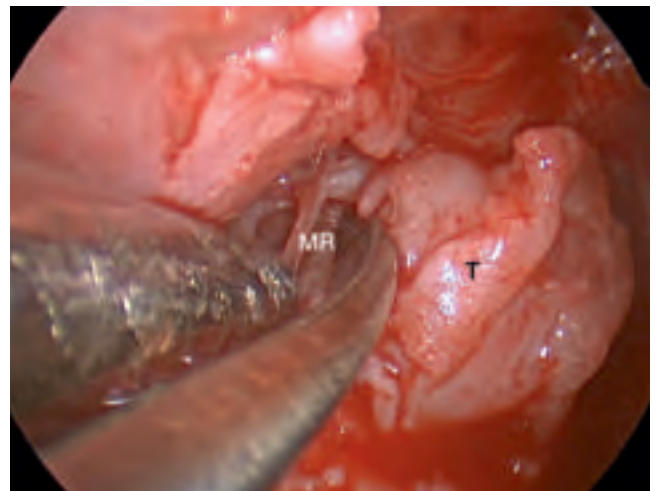


**Fig. 6.56** The tumor (T) is resected from the medial wall of the orbit. The medial rectus (MR) muscle fibers are seen underneath.

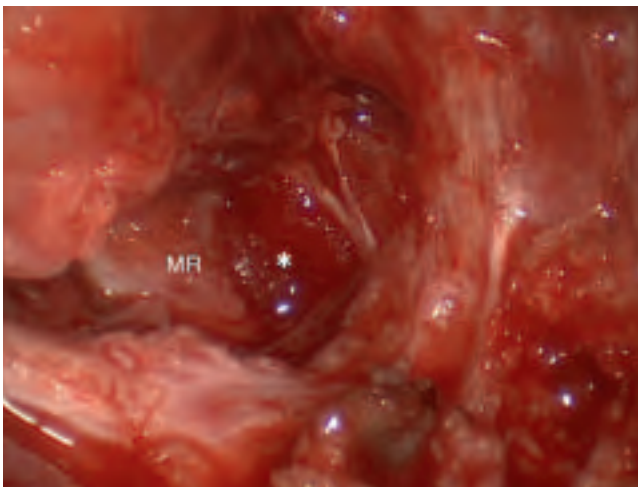


**Fig. 6.57** A small piece of Gelfoam (\*) is placed in the resection cavity and the procedure is completed. Medial rectus (MR).

## 6.8 Transpterygoid Approach for Juvenile Nasopharyngeal Angiofibroma (JNA)



**Fig. 6.58** Transpterygoid approach using the transmaxillary corridor.

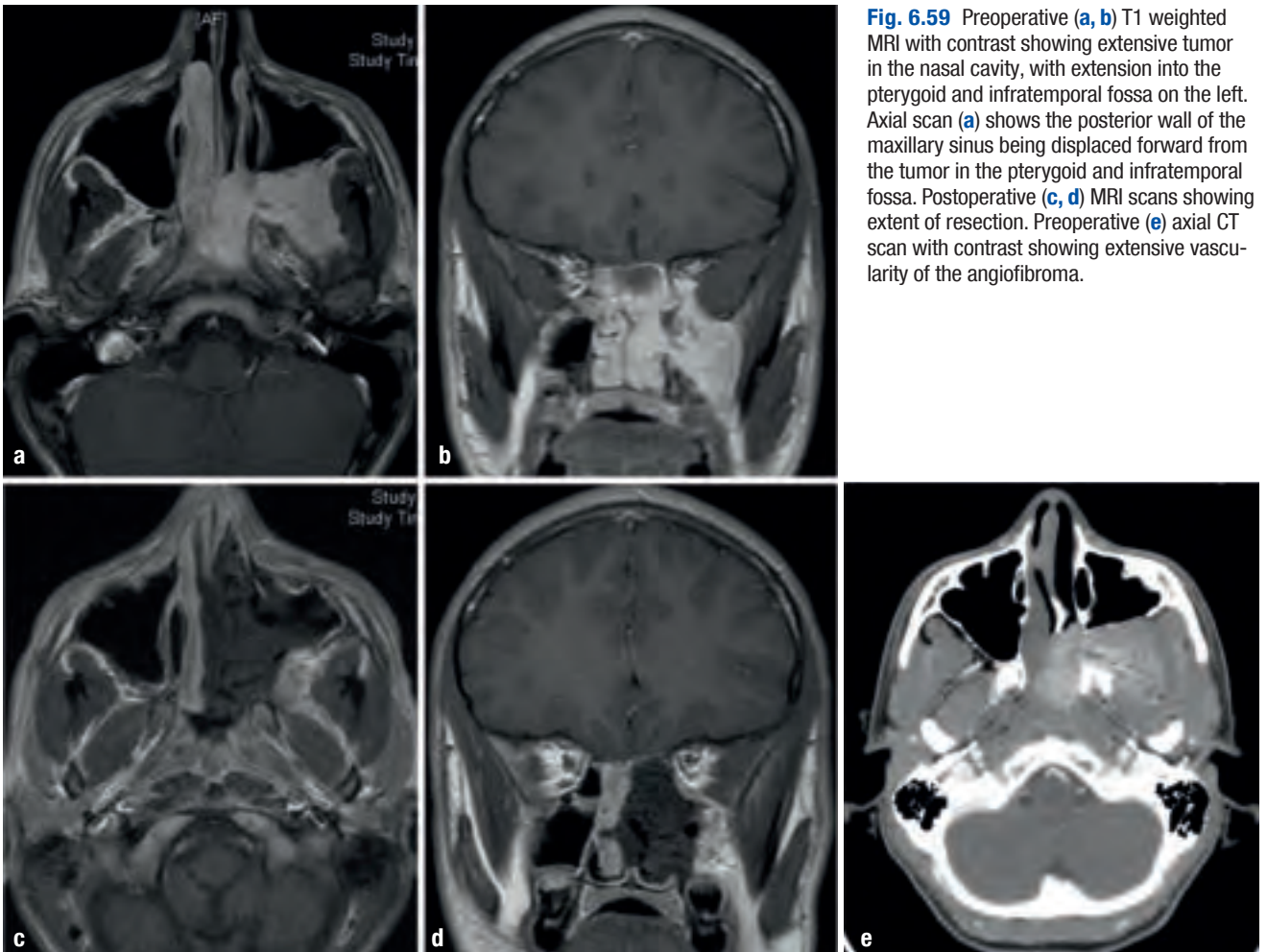


**Fig. 6.59** Preoperative (a, b) T1 weighted MRI with contrast showing extensive tumor in the nasal cavity, with extension into the pterygoid and infratemporal fossa on the left. Axial scan (a) shows the posterior wall of the maxillary sinus being displaced forward from the tumor in the pterygoid and infratemporal fossa. Postoperative (c, d) MRI scans showing extent of resection. Preoperative (e) axial CT scan with contrast showing extensive vascularity of the angiofibroma.

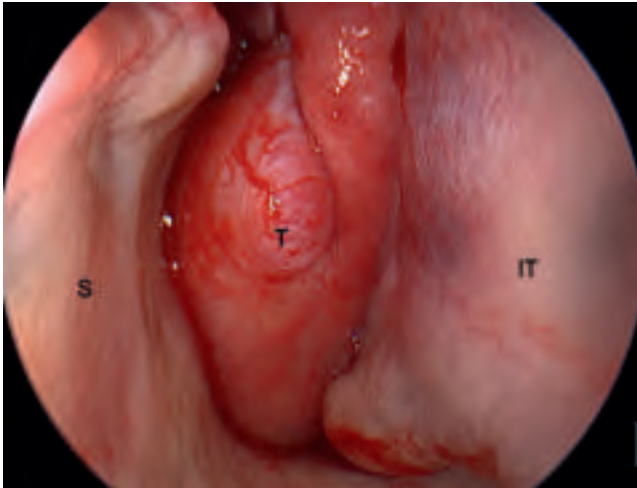


**Fig. 6.60** The vascular tumor (T) is seen growing into the nasal cavity. Septum (S); inferior turbinate (IT).

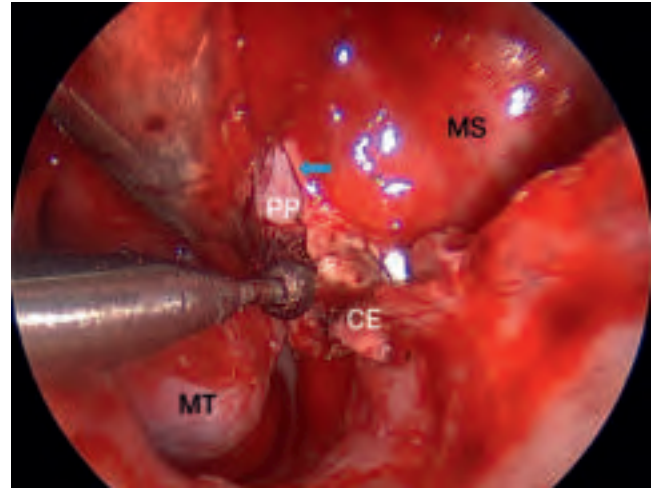


**Fig. 6.61** The maxillary sinus ostium lateral to the medial turbinate (MT) is entered and enlarged, revealing the posterior wall of the maxillary sinus (MS). The medial and lateral posterior wall of the maxillary sinus forms the anterior wall of the pterygopalatine fossa and infratemporal fossa respectively. Removing the posterior plate of the palatine bone (PP) exposes the pterygopalatine fossa (←). The sphenopalatine artery is identified, coagulated and divided. Crista ethmoidalis (CE).

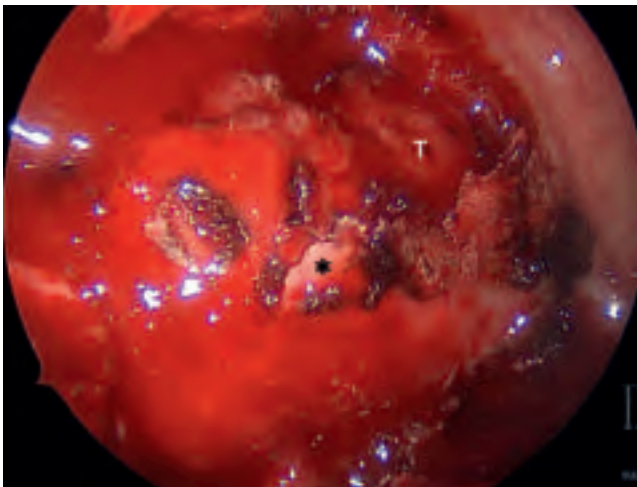


**Fig. 6.62** The posterior wall of the maxillary sinus (\*) has bony dehiscence from tumor (T) pushing into the maxillary sinus from the infratemporal fossa.

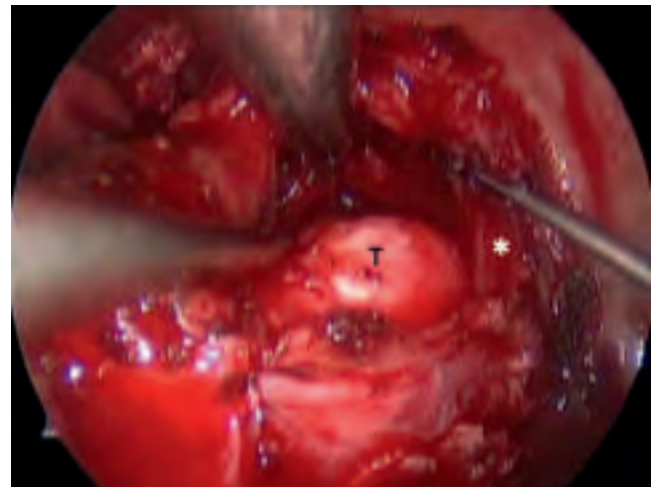


**Fig. 6.63** The posterior wall of the maxillary sinus is removed. The tumor (T) is dissected free superiorly from the infratemporal fossa. Ascending ramus (\*) of mandible on the left.



**Fig. 6.64** Lateral dissection of tumor from the infratemporal fossa.

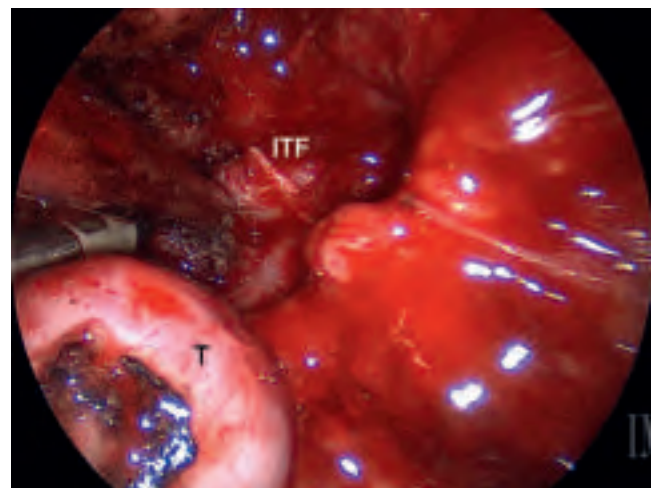


**Fig. 6.65** The tumor (T) is removed revealing the floor of the infratemporal fossa (ITF).

## Recommended Reading

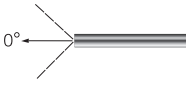
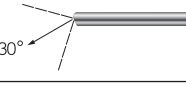
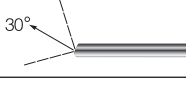
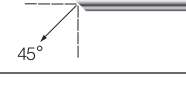
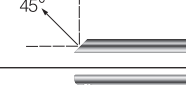
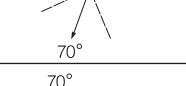
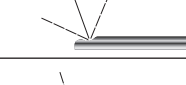
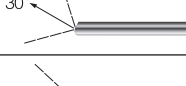
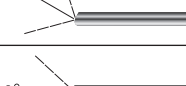
1. BANU MA, GUERRERO-MALDONADO A, MCCREA HJ, GARCIA-NAVARRO V, SOUWEIDANE MM, ANAND VK ET AL. Impact of skull base development on endonasal endoscopic surgical corridors. *J Neurosurg Pediatr* 2014;13(2):155–69. doi:10.3171/2013.10.PEDS13303.
2. BANU MA, RATHMAN A, PATEL KS, SOUWEIDANE MM, ANAND VK, GREENFIELD JP ET AL. Corridor-based endonasal endoscopic surgery for pediatric skull base pathology with detailed radioanatomic measurements. *Neurosurgery* 2014;10 Suppl 2:273-93; discussion 293. doi:10.1227/NEU.0000000000000252.
3. CAICEDO-GRANADOS E, CARRAU R, SNYDERMAN CH, PREVEDELLO D, FERNANDEZ-MIRANDA J, GARDNER P ET AL. Reverse rotation flap for reconstruction of donor site after vascular pedicled nasoseptal flap in skull base surgery. *Laryngoscope* 2010;120(8):1550–2. doi:10.1002/lary.20975.
4. CHIVUKULA S, KOUTOUROUSIOU M, SNYDERMAN CH, FERNANDEZ-MIRANDA JC, GARDNER PA, TYLER-KABARA EC. Endoscopic endonasal skull base surgery in the pediatric population. *J Neurosurg Pediatr* 2013;11(3):227–41. doi:10.3171/2012.10.PEDS12160.
5. GHOSH A, HATTEN K, LEARNED KO, RIZZI MD, LEE JY, STORM PB ET AL. Pediatric nasoseptal flap reconstruction for suprasellar approaches. *Laryngoscope* 2015;125(11):2451–6. doi:10.1002/lary.25395.
6. GÜLDNER C, PISTORIUS SM, DIOGO I, BIEN S, SESTERHENN A, WERNER JA. Analysis of pneumatization and neurovascular structures of the sphenoid sinus using cone-beam tomography (CBT). *Acta Radiol* 2012;53(2):214–9. doi:10.1258/ar.2011.110381.
7. KHALILI S, PALMER JN, ADAPPA ND. The expanded endonasal approach for the treatment of intracranial skull base disease in the pediatric population. *Curr Opin Otolaryngol Head Neck Surg* 2015;23(1):65–70. doi:10.1097/MOO.0000000000000126.
8. LOCATELLI D, MASSIMI L, RIGANTE M, CUSTODI V, PALUDETTI G, CASTELNUOVO P ET AL. Endoscopic endonasal transsphenoidal surgery for sellar tumors in children. *Int J Pediatr Otorhinolaryngol* 2010;74(11):1298–302. doi:10.1016/j.ijporl.2010.08.009.
9. MA J, HUANG Q, LI X, HUANG D, XIAN J, CUI S ET AL. Endoscopic transnasal repair of cerebrospinal fluid leaks with and without an encephalocele in pediatric patients: from infants to children. *Childs Nerv Syst* 2015;31(9):1493–8. doi:10.1007/s00381-015-2746-y.
10. MCCREA HJ, GEORGE E, SETTLER A, SCHWARTZ TH, GREENFIELD JP. Pediatric Suprasellar Tumors. *J Child Neurol* 2015. doi:10.1177/0883073815620671.
11. RASTATTER JC, SNYDERMAN CH, GARDNER PA, ALDEN TD, TYLER-KABARA E. Endoscopic endonasal surgery for sinonasal and skull base lesions in the pediatric population. *Otolaryngol Clin North Am* 2015;48(1):79–99. doi:10.1016/j.otc.2014.09.007.
12. SCHWARTZ TH, FRASER JF, BROWN S, TABAEE A, KACKER A, ANAND VK. Endoscopic cranial base surgery: classification of operative approaches. *Neurosurgery* 2008;62(5):991-1002; discussion 1002-5. doi:10.1227/01.neu.0000325861.06832.06.
13. TSAI EC, SANTORENEOS S, RUTKA JT. Tumors of the skull base in children: review of tumor types and management strategies. *Neurosurg Focus* 2002;12(5):e1. doi:10.3171/foc.2002.12.5.2.
14. WANG J, BIDARI S, INOUE K, YANG H, RHOTON A. Extensions of the sphenoid sinus: a new classification. *Neurosurgery* 2010;66(4):797–816. doi:10.1227/01.NEU.0000367619.24800.B1.
15. YOUSSEF CA, SMOTHERMAN CR, KRAEMER DF, ALDANA PR. Predicting the limits of the endoscopic endonasal approach in children: a radiological anatomical study. *J Neurosurg Pediatr* 2016;17(4):510–5. doi:10.3171/2015.6.PEDS14695.

## **Recommended Instrumentation and Video Equipment for Pediatric Endonasal Endoscopic Skull Base Surgery**

## Straight Telescopes



**HOPKINS® Telescopes, autoclavable,**  
with connection for fiber optic light cable on upper side,  
fiber optic light transmission incorporated,  
color-coded according to direction of view

Direction of View	Order No.	Outer Diameter	Length
	28132 AA	4 mm	18 cm
	28132 BA		
	28132 BVA		
	28132 FA		
	28132 FVA		
	28132 CA		
	28132 CVA		
	28132 BWA		
	28164 AA	30 cm	
	28164 BA		
	28018 AA	2.7 mm	18 cm

It is recommended to check the suitability of the product for the intended procedure prior to use.

## EndoCAMeleon® NEURO HOPKINS® Telescope

The ENDOCAMELEON® is the latest addition to the HOPKINS® product family of rod lens telescopes – and by far the most versatile.

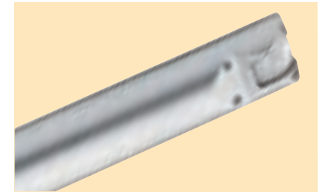
With a simple turn of the control dial, the ENDOCAMELEON® enables the user to easily select the direction of view between 15° and 90°. Consequently, the surgeon can quickly and easily select the direction of view that provides optimal orientation and control in any situation.

The ENDOCAMELEON® from KARL STORZ takes the endoscopic OR to a new quality level as it noticeably improves orientation during an intervention – without the time-consuming changeover between several telescopes – and thus enables safe and smooth surgery.

The ENDOCAMELEON® combines the user comfort of the proven HOPKINS® endoscopes with unprecedented versatility – offering the high quality associated with KARL STORZ telescopes.

### Special Features:

- Variable direction of view (15° to 90°)
- Easy-to-use control dial for selecting the direction of view
- Lightweight and modern design
- HOPKINS® telescope with unique rod lens system
- Diameter 4 mm, length 18 cm
- Standard eyepiece fits any camera head



The familiar ergonomics and handling of conventional telescopes are now complemented by the convenience of a variable direction of view



The direction of view is changed using the control dial at the proximal end of the ENDOCAMELEON®

## Telescope



28132 AE **ENDOCAMELEON® NEURO HOPKINS® Telescope**, diameter 4 mm, length 18 cm, **autoclavable**, variable direction of view from 15°–90°, adjustment knob for selecting the desired direction of view, fiber optic light transmission incorporated, color code: gold



7230 AES **Irrigation and Suction Sheath**, outer diameter 4.8 x 6 mm, working length 14 cm, for use with ENDOCAMELEON® HOPKINS® Telescope and KARL STORZ lens irrigation system CLEARVISION® II

## Coagulation



### TAKE-APART® Bipolar Forceps

	Order No.	Description	Width of Jaws	Working Length
	28164 BDB	<b>TAKE-APART® Bipolar Forceps</b> , short, rounded tip, outer diameter 3.4 mm	2 mm	14 cm
	28164 BDC	<b>TAKE-APART® Bipolar Forceps</b> , short, outer diameter 3.4 mm		
	28164 BDN	<b>TAKE-APART® Bipolar Forceps</b> , rounded tip, outer diameter 3.4 mm	2 mm	20 cm
	28164 BDM	<b>TAKE-APART® Bipolar Forceps</b> , with fine jaws, distally angled 45°, horizontal closing, outer diameter 3.4 mm	1 mm	
	28164 BDD	<b>TAKE-APART® Bipolar Forceps</b> , distally angled 45°, horizontal closing, outer diameter 3.4 mm	2 mm	
	28164 BDK	<b>TAKE-APART® Bipolar Forceps</b> , distally angled 45°, horizontal closing, size 3.4 mm	4 mm	
	28164 BDL	<b>TAKE-APART® Bipolar Forceps</b> , with fine jaws, distally angled 45°, vertical closing, outer diameter 3.4 mm	1 mm	
	28164 BDG	<b>TAN TAKE-APART® Bipolar Coagulation Forceps</b> , size 3.4 mm	3 mm	
	26176 LV	<b>Bipolar High Frequency Cord</b> , for KARL STORZ AUTOCON® II 400 SCB system (112, 114, 116, 122, 125), AUTOCON® II 200, AUTOCON® II 80 and Valleylab coagulator	–	
	26176 LW	<b>Bipolar High Frequency Cord</b> , pin distance on unit side 22 mm, for use with high frequency surgical units with bipolar sockets with 22 mm pin distance	–	300 cm



**Bipolar Forceps**

	Order No.	Description	Width of Jaws	Working Length
	28164 BGK	<b>Bipolar Forceps</b> , jaws curved upwards 45°, for bipolar coagulation in skull base and pituitary surgery	–	18 cm
	847002 V	<b>Bipolar High Frequency Cord</b> , for AUTOCON® II 400 SCB system (112, 114, 116), Valleylab coagulator, with two 2 mm cable sockets for bipolar suction forceps	–	450 cm



**Bipolar Coagulation Ball Electrodes\***

	Order No.	Description	Diameter	Working Length
	28164 ED	<b>Coagulation Ball Electrode</b> , laterally curved	2 mm	13 cm
	28164 EF	<b>Coagulation Ball Electrode</b> , laterally curved	4 mm	

\* Available Unipolar High Frequency Cords (26002 M, 26004 M, 26005 M, 26006 M) are selected in accordance with the generator used. Please refer to the KARL STORZ product catalog for more detailed information.



### Bipolar Coagulation Forceps

	Order No.	Description	Tip	Working Length
	28164 BPA	<b>Bipolar Coagulation Forceps</b> , insulated, bayonet-shaped, blunt, total length 23 cm	0.7 mm	12 cm
	28164 BPB	<b>Bipolar Coagulation Forceps</b> , insulated, bayonet-shaped, blunt, total length 25 cm		14 cm
	28164 BPC	<b>Bipolar Coagulation Forceps</b> , insulated, bayonet-shaped, blunt, total length 23 cm	0.3 mm	12 cm
	847000 V	<b>Bipolar High Frequency Cord</b> , for KARL STORZ AUTOCON® II 400 SCB systems (112, 114, 116, 122, 125), Valleylab coagulator and KARL STORZ bipolar coagulation forceps	–	300 cm
	847000 W	<b>Bipolar High Frequency Cord</b> , pin distance on the unit side 22 mm, for use with HF units with bipolar sockets with 22 mm pin distance and KARL STORZ bipolar coagulation forceps	–	300 cm

### KERRISON Bone Punches



KERRISON Bone Punches

	Order No.	Description	Diameter	Working Length
	28164 MKA	<b>Bone Punch</b> , detachable, rigid, upbiting 60° forward	1 mm	17 cm
	28164 MKB		2 mm	
	28164 MKC		3 mm	
	28164 MKK		4 mm	
	28164 MKL		5 mm	
	28164 MKD	<b>Bone Punch</b> , detachable, rigid, downbiting 60° forward	1 mm	
	28164 MKE		2 mm	
	28164 MKF		3 mm	
	28164 MKO		4 mm	

## Curettes, Dissectors, Hooks and Knives

### Spoon Curettes



#### Curettes

	Order No.	Description	Size	Length
	28164 KA	<b>Curette</b> , round spoon, with round handle	1 mm	25 cm
	28164 KB		2 mm	
	28164 KC		3 mm	
	28164 KF		2 mm	
	28164 KG		3 mm	
	28164 KLA	<b>Spoon Curette</b> , straight, working length 13 cm	1 mm	23 cm
	28164 KLB	<b>Spoon Curette</b> , angled 45°, working length 13 cm		
	28164 KLC	<b>Spoon Curette</b> , angled 90°		
	28164 KLD	<b>Spoon Curette</b> , straight, round handle, working length 13 cm	0.8 mm	
	28164 KLE	<b>Spoon Curette</b> , angled 45°, round handle, working length 13 cm		
	28164 KLF	<b>Spoon Curette</b> , angled 90°, round handle, working length 13 cm		
	28164 KLG	<b>Spoon Curette</b> , straight, working length 13 cm	2 mm	
	28164 KLH	<b>Spoon Curette</b> , angled 45°, working length 13 cm		
	28164 KLI	<b>Spoon Curette</b> , angled 90°, working length 13 cm		



#### Ring Curettes

	Order No.	Description	Inner Dia.	Length
	28164 RN	<b>Ring Curette</b> , with round wire, tip angled 45°, with round handle	3 mm	25 cm
	28164 RO		5 mm	
	28164 RP		7 mm	
	28164 RE	<b>Ring Curette</b> , with round wire, malleable, tip angled 45°, with round handle	3 mm	
	28164 RJ		5 mm	
	28164 RK		7 mm	

	Order No.	Description	Inner Dia.	Length
	28164 RI	<b>Ring Curette</b> , with round wire, tip angled 90°, with round handle	3 mm	25 cm
	28164 RG		5 mm	
	28164 RH		7 mm	
	28164 RB	<b>Ring Curette</b> , with round wire, laterally curved sheath end, with round handle	3 mm	
	28164 RA		5 mm	
	28164 RC		7 mm	
	28164 RV	<b>Ring Curette</b> , with round wire, laterally curved sheath end 90°, with round handle	3 mm	
	28164 RD		5 mm	
	28164 RW		7 mm	
	28164 RR	<b>Curette, blunt</b> , stirrup-shaped, with round handle	–	



CAPPABIANCA-de DIVITIIS Ring Currettes

	Order No.	Description	Outer Dia.	Working Length
	28164 RF	<b>Ring Curette</b> , with round wire, vertical, with round handle	5 mm	25 cm
	28164 RFL		7 mm	
	28164 RM	<b>Ring Curette</b> , with round wire, horizontal, with round handle	5 mm	
	28164 RML		7 mm	



FRANK-PASQUINI Ring Currettes

	Order No.	Description	Outer Dia.	Working Length
	28164 FRA	<b>Ring Curette</b> , distal end curved, vertical	2.6 mm	15 cm
	28164 FRC		5 mm	
	28164 FRE		7 mm	
	28164 FRB	<b>Ring Curette</b> , distal end curved, horizontal	2.6 mm	
	28164 FRD		5 mm	
	28164 FRF		7 mm	



### Sharp Dissectors

	Order No.	Description	Width	Length	
	28164 DA	<b>Dissector</b> , sharp, tip angled 45°, round spatula, with round handle	2 mm	25 cm	
	28164 DB		3 mm		
	28164 DF	<b>Dissector</b> , sharp, tip angled 15°, flat long spatula, with round handle	1.5 mm		
	28164 DG		2 mm		
	28164 DT	<b>Dissector</b> , sharp, slightly curved spatula, tip angled 15°, with round handle	1 mm		
	28164 DM	<b>Dissector</b> , sharp, slightly curved spatula, straight, with round handle	3 mm		
	28164 DS	<b>Dissector</b> , sharp, tip angled 15°, with round handle	2 mm		
	28164 DLA	<b>Dissector</b> , tip angled 15°, working length 13 cm	1 mm		23 cm
	28164 DLB	<b>Dissector</b> , tip angled 45°, working length 13 cm			
	28164 DLC	<b>Dissector</b> , tip angled 90°, working length 13 cm			
	28164 DLD	<b>Dissector</b> , tip angled 15°, working length 13 cm	0.5 mm		
	28164 DLE	<b>Dissector</b> , tip angled 45°, working length 13 cm			
	28164 DLF	<b>Dissector</b> , tip angled 90°, working length 13 cm			



**CASTELNUOVO Hooks**

	Order No.	Description	Width	Length
	28164 H	<b>Hook, 90°</b> , blunt, with round handle	-	25 cm
	28164 HA	<b>Seeker, angled 45°</b>	1 mm	
	28164 HB	<b>Seeker, angled 90°</b>	0.4 mm	
	28164 HC	<b>Seeker, angled 90°</b>	1 mm	



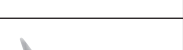
**de DIVITIIS-CAPPABIANCA Scalpels**

	Order No.	Description
	28164 M	de DIVITIIS-CAPPABIANCA <b>Scalpel</b> , with retractable blade
	28164 KK	de DIVITIIS-CAPPABIANCA <b>Scalpel</b> , with retractable blade

## Scissors



### Scissors

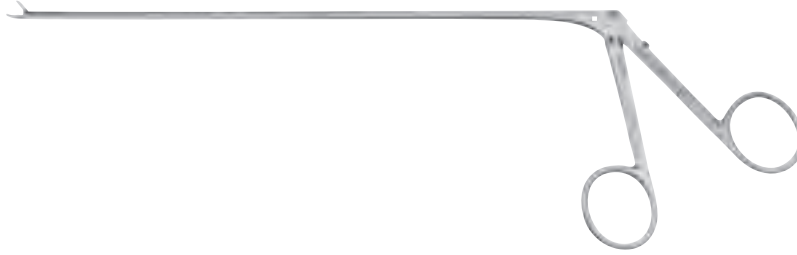
	Order No.	Description	Working Length
	28164 MZB	<b>Scissors</b> , straight, with small handle, with cleaning connector	18 cm
	28164 MZC	<b>Scissors</b> , curved to right, with small handle, with cleaning connector	
	28164 MZD	<b>Scissors</b> , curved to left, with small handle, with cleaning connector	
	28164 MZE	<b>Scissors</b> , angled upwards, with small handle, with cleaning connector	
	28164 SAD	<b>Scissors</b> , upturned 45°, delicate, sheath 360° rotatable, with cleaning connector	



### SEPEHRNIA Micro Scissors

	Order No.	Description	Working Length
	28164 SBA	<b>Micro Scissors</b> , bayonet-shaped, sharp/sharp, straight	10 cm
	28164 SBB	<b>Micro Scissors</b> , bayonet-shaped, sharp/sharp, curved to left	
	28164 SBC	<b>Micro Scissors</b> , bayonet-shaped, blunt/blunt, jaw straight	
	28164 SBD	<b>Micro Scissors</b> , bayonet-shaped, sharp/sharp, jaw curved to right	
	28164 SBE	<b>Micro Scissors</b> , bayonet-shaped, sharp/sharp, jaw horizontal	

## Forceps



### Double Spoon Miniature Forceps

	Order No.	Description	Spoon Dia.	Working Length
	28164 TD	<b>Forceps</b> , round cupped jaws, extra delicate, straight	0.6 mm	18 cm
	28164 T	<b>Forceps</b> , oval cupped jaws, extra delicate, straight	0.9 mm	
	28164 TA	<b>Forceps</b> , oval cupped jaws, extra delicate, upturned		
	28164 TE	<b>Forceps</b> , oval cupped jaws, extra delicate, curved to right	0.6 mm	
	28164 TF	<b>Forceps</b> , oval cupped jaws, extra delicate, curved to left		



### Cutting Forceps

	Order No.	Description	Spoon Dia.	Working Length
	28164 MZF	<b>Spoon Forceps</b> , single action jaws	3 x 10 mm	17 cm



### SEPEHRNIA Spoon Forceps

	Order No.	Description	Spoon Dia.	Working Length
	28164 PBB	<b>Micro Forceps</b> , bayonet-shaped	2 mm	10 cm
	28164 PBE		4 mm	
	28164 PBF		6 mm	
	28164 PBG	<b>Micro Forceps</b> , bayonet-shaped, spoon horizontal	2 mm	
	28164 PBH		4 mm	
	28164 PBI		6 mm	



### SEPEHRNIA Spoon Forceps

	Order No.	Description	Size	Working Length
	28164 PBA	<b>Micro Grasping Forceps</b> , bayonet-shaped, straight jaws, smooth	0.5 mm	10 cm
	28164 PBC	<b>Micro Grasping Forceps</b> , bayonet-shaped, straight jaws, serrated	3 mm	
	28164 PBD	<b>Micro Grasping Forceps</b> , bayonet-shaped, jaws curved to left	0.75 mm	



### Grasping Forceps

	Order No.	Description	Size	Working Length
	28164 MZA	<b>Grasping Forceps</b> , fine serration, straight, with cleaning connector	–	18 cm



### Miniature Grasping Forceps

	Order No.	Description	Size	Working Length
	28164 GF	<b>Miniature Grasping Forceps</b> , serrated, straight	–	18 cm



**Miniature Forceps, through-cutting**

	Order No.	Description	Bite	Working Length
	28164 GS	<b>Miniature Forceps,</b> straight, through-cutting, with fine flat jaws	1 mm	18 cm
	28164 GR	<b>Miniature Forceps,</b> curved to right, through-cutting, with fine flat jaws		
	28164 GL	<b>Miniature Forceps,</b> curved to left, through-cutting, with fine flat jaws		
	28164 GU	<b>Miniature Forceps,</b> curved upwards, through-cutting, with fine flat jaws		

**RHINOFORCE® II, through-cutting**

	Order No.	Description	Bite	Working Length
	28164 UA	<b>RHINOFORCE® II Nasal Forceps,</b> with extra fine flat jaws, through-cutting, tissue-sparing, straight sheath, straight jaws, with cleaning connector	1.5 mm	18 cm
	28164 UB	<b>RHINOFORCE® II Nasal Forceps,</b> with extra fine flat jaws, through-cutting, tissue-sparing, straight sheath, jaws angled upwards 45°, with cleaning connector		
	28164 UE	<b>RHINOFORCE® II Nasal Forceps,</b> with extra fine flat jaws, through-cutting, tissue-sparing, straight sheath, jaws angled downwards 45°, with cleaning connector		
	28164 UD	<b>RHINOFORCE® Nasal Forceps,</b> with extra fine, flat jaws, through-cutting, tissue-sparing, sheath end curved upwards 25°, jaws angled downwards 45°		

# IMAGE1 S Camera System <sup>NEW</sup>



Economical and future-proof

- Modular concept for flexible, rigid and 3D endoscopy as well as new technologies
- Forward and backward compatibility with video endoscopes and FULL HD camera heads

- Sustainable investment
- Compatible with all light sources



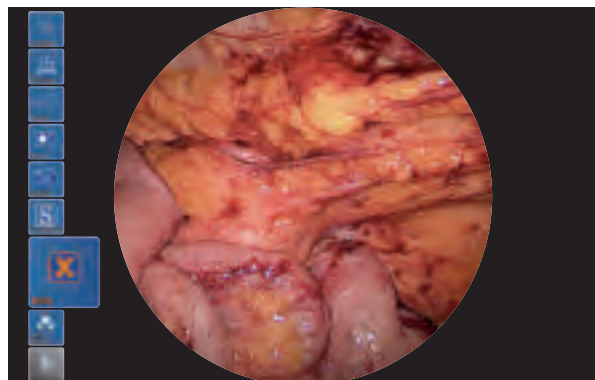
Innovative Design

- Dashboard: Complete overview with intuitive menu guidance
- Live menu: User-friendly and customizable
- Intelligent icons: Graphic representation changes when settings of connected devices or the entire system are adjusted

- Automatic light source control
- Side-by-side view: Parallel display of standard image and the Visualization mode
- Multiple source control: IMAGE1 S allows the simultaneous display, processing and documentation of image information from two connected image sources, e.g., for hybrid operations



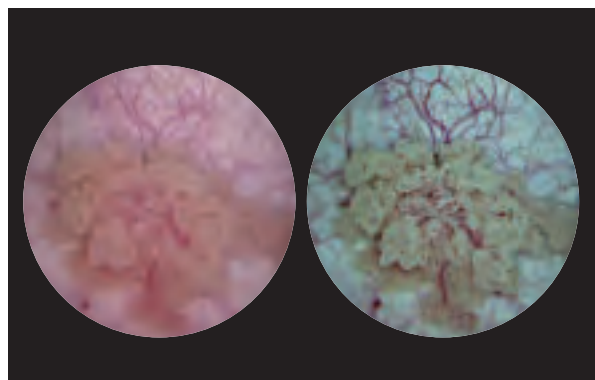
Dashboard



Live menu



Intelligent icons



Side-by-side view: Parallel display of standard image and Visualization mode

## IMAGE1 S Camera System <sup>NEW</sup>

# IMAGE1 S

### Brilliant Imaging

- Clear and razor-sharp endoscopic images in FULL HD
- Natural color rendition

- Reflection is minimized
- Multiple IMAGE1 S technologies for homogeneous illumination, contrast enhancement and color shifting



FULL HD image



CLARA



FULL HD image



CHROMA



FULL HD image



SPECTRA A\*



FULL HD image



SPECTRA B\*\*

\* SPECTRA A: Not for sale in the U.S.

\*\* SPECTRA B: Not for sale in the U.S.

# IMAGE1 S Camera System <sup>NEW</sup>



TC 200EN

TC 200EN\* **IMAGE1 S CONNECT**, connect module, for use with up to 3 link modules, resolution 1920 x 1080 pixels, with integrated KARL STORZ-SCB and digital Image Processing Module, power supply 100–120 VAC/200–240 VAC, 50/60 Hz including:  
**Mains Cord**, length 300 cm  
**DVI-D Connecting Cable**, length 300 cm  
**SCB Connecting Cable**, length 100 cm  
**USB Flash Drive**, 32 GB, USB silicone keyboard, with touchpad, US  
**\* Available in the following languages:** DE, ES, FR, IT, PT, RU

**Specifications:**

HD video outputs	- 2x DVI-D - 1x 3G-SDI
Format signal outputs	1920 x 1080p, 50/60 Hz
LINK video inputs	3x
USB interface	4x USB, (2x front, 2x rear)
SCB interface	2x 6-pin mini-DIN

Power supply	100–120 VAC/200–240 VAC
Power frequency	50/60 Hz
Protection class	I, CF-Defib
Dimensions w x h x d	305 x 54 x 320 mm
Weight	2.1 kg

**For use with IMAGE1 S  
IMAGE1 S CONNECT Module TC 200EN**



TC 300

TC 300 **IMAGE1 S H3-LINK**, link module, for use with IMAGE1 FULL HD three-chip camera heads, power supply 100–120 VAC/200–240 VAC, 50/60 Hz, **for use with IMAGE1 S CONNECT TC 200EN** including:  
**Mains Cord**, length 300 cm  
**Link Cable**, length 20 cm

**Specifications:**

<b>Camera System</b>	<b>TC 300 (H3-Link)</b>
Supported camera heads/video endoscopes	TH 100, TH 101, TH 102, TH 103, TH 104, TH 106 (fully compatible with IMAGE1 S) <b>22220055-3, 22220056-3, 22220053-3, 22220060-3, 22220061-3, 22220054-3, 22220085-3</b> (compatible without IMAGE1 S technologies CLARA, CHROMA, SPECTRA*)
LINK video outputs	1x
Power supply	100–120 VAC/200–240 VAC
Power frequency	50/60 Hz
Protection class	I, CF-Defib
Dimensions w x h x d	305 x 54 x 320 mm
Weight	1.86 kg

\* SPECTRA A: Not for sale in the U.S.  
 \*\* SPECTRA B: Not for sale in the U.S.

## IMAGE1 S Camera Heads <sup>NEW</sup>

# IMAGE1 S

For use with IMAGE1 S Camera System

IMAGE1 S CONNECT Module TC 200EN, IMAGE1 S H3-LINK Module TC 300  
and with all IMAGE1 HUB™ HD Camera Control Units



TH 100

TH 100

**IMAGE1 S H3-Z Three-Chip FULL HD Camera Head,**  
50/60 Hz, IMAGE1 S compatible, progressive scan,  
soakable, gas- and plasma-sterilizable, with integrated  
Parfocal Zoom Lens, focal length  $f = 15-31$  mm (2x),  
2 freely programmable camera head buttons,  
for use with IMAGE1 S and IMAGE1 HUB™ HD/HD

### Specifications:

IMAGE1 FULL HD Camera Heads	IMAGE1 S H3-Z
Product no.	TH 100
Image sensor	3x 1/8" CCD chip
Dimensions w x h x d	39 x 49 x 114 mm
Weight	270 g
Optical interface	integrated Parfocal Zoom Lens, $f = 15-31$ mm (2x)
Min. sensitivity	F 1.4/1.17 Lux
Grip mechanism	standard eyepiece adaptor
Cable	non-detachable
Cable length	300 cm



TH 104

TH 104

**IMAGE1 S H3-ZA Three-Chip FULL HD Camera Head,**  
50/60 Hz, IMAGE1 S compatible, **autoclavable**,  
progressive scan, soakable, gas- and plasma-sterilizable,  
with integrated Parfocal Zoom Lens, focal length  
 $f = 15-31$  mm (2x), 2 freely programmable camera head  
buttons, for use with IMAGE1 S and IMAGE1 HUB™ HD/HD

### Specifications:

IMAGE1 FULL HD Camera Heads	IMAGE1 S H3-ZA
Product no.	TH 104
Image sensor	3x 1/8" CCD chip
Dimensions w x h x d	39 x 49 x 100 mm
Weight	299 g
Optical interface	integrated Parfocal Zoom Lens, $f = 15-31$ mm (2x)
Min. sensitivity	F 1.4/1.17 Lux
Grip mechanism	standard eyepiece adaptor
Cable	non-detachable
Cable length	300 cm



